QATAR UNIVERSITY

COLLEGE OF ENGINEERING

THERMAL COMFORT CONDITIONS OF AN INDOOR SWIMMING POOL

BY

HOUSSAMELDIN MOHAMED HASSANIN MOHAMED HASSANIN MESLAM

A Thesis Submitted to

the College of Engineering

in Partial Fulfillment of the Requirements for the Degree of

Master of Science in Mechanical Engineering

[January] 2023

COMMITTEE PAGE

The members of the Committee approve the Thesis of
Houssameldin defended on 01/01/2023.

Samer Ahmed
Thesis/Dissertation Supervisor

Ahmad Sleiti
Committee Member

–

Approved:

Khalid Kamal Naji, Dean, College of Engineering

ABSTRACT

MESLAM, HOUSSAMELDIN, M., Masters : January : 2023, Masters of Science in Mechanical Engineering

Title: Studying Thermal Comfort Conditions Of An Indoor Swimming Pool

Supervisor of Thesis: Samer, F., Ahmed .

In this thesis, the thermal comfort and indoor conditions for an indoor swimming pool located in desert climate are investigated numerically. Such climate is characterized by very mild winters, and very hot and sunny summers such as in Qatar. A 17.6 m x 11.7 m indoor swimming pool was studied for an outdoor summer condition of 43.3 ℃ dry-bulb temperature (DBT) and 33.3 ℃ wet bulb temperature (WBT) and for outdoor winter condition of 17 ℃ DBT and 10.6 ℃ WBT. The required design indoor temperatures were taken as 24-29 ℃ all year round and the relative humidity within 50-60% in summer and 40-60% in winter according to ASHRAE Handbook applications (Chapter 6: Indoor Swimming Pools). The calculated pool evaporation rate was 0.005565 kg/s corresponding to latent heat load gain of 13.5 Kw (3.8 TR) to the swimming pool space. Using HAP carrier software, the calculated total thermal load was 61.9 kW (17.6 TR) that needs to be removed from the pool envelope using 1.610 kg/s air flow in summer and 0.560 kg/s in winter. Computational Fluid Dynamics (CFD) simulations were conducted via Ansys Fluent 19.2 1to investigate the recommended indoor conditions limits using standard K-□ model for turbulence modeling and species transport model for moisture content calculations. A grid independence study was conducted and the final grid consisted of 1869824 elements and 1.2 growth rate. The result of numerical calculation showed the following average

values in summer: 24 ℃ air temperature, 0.4 m/s air velocity and 47.7% relative humidity. On the other hand, 24.1℃ air temperature, 0.4 m/s air velocity and 42.1% relative humidity were determined as the average air flow variables in winter season. The results of the numerical calculations were employed in Fanger's thermal comfort model to analyze the thermal comfort sensation of human in the swimming pool space at several heights (y=0.1, 0.6, 1.1 and 1.7 m). The predicted mean vote (PMV) and the predicted percentage of dissatisfied (PPD) are the two indictors that were used in assessing the thermal comfort of occupant. In summer, it was found that people would feel comfortable as the calculated PMV was +0.13 indicting a nearly neutral sensation neither cold nor hot. PPD showed that 5.5% only of occupants felt dissatisfied from the indoor conditions of the swimming pool. PMV of +0.73 indicated slightly warm sensation for people occupying the space in winter season. 84% of occupant felt satisfied while 16% sensed dissatisfied as per the numerical results of indoor condition in winter. The methodology and the results presented in this thesis work can serve as reputable reference and guide for future research related to challenging designs of swimming pools and green houses in desert regions.

DEDICATION

A special thanking to my parents, supervisors and friends without them, I would not be able to reach to this level in my academic path.

ACKNOWLEDGMENTS

I would like to thank all the QU students and staff who supported me during my academic study in Master degree. I would like to express my appreciation to my thesis supervisor Prof. Samer Ahmed and Prof. Ahmad Sleiti, they presented a great opportunity to me as master student working on my master thesis under their supervision and guidance.

TABLE OF CONTENTS

LIST OF TABLES

LIST OF FIGURES

CHAPTER 1: INTRODUCTION

1.1 Background

Studying thermal performance of facilities using Air conditioning system is valuable as it does affect the efficiency of people in their daily activities. Comfort is important measure of people's efficiency which is affected by their activity level, type of cloth, indoor condition and outdoor environment. Using high energy consumption to remove thermal loads from buildings was adopted as a concept in achieving thermal comfort in HVAC industry. High energy consumption of cooling equipment does not insure achieving thermal comfort as comfort depends on specific air variable limitations as described in Franger's model (section 3.4 thermal comfort indices). In addition, HVAC engineers are using area/cooling load factor without basis to estimate cooling loads which leads to an overestimation of envelop thermal loads. Therefore, Proper thermal load and thermal comfort analysis required to be conducted to achieve the optimum balance between energy consumption and thermal comfort. Recently, it has shown to be one of the major problems in HVAC applications that air conditioning system was unable to do its function through supplying comfort measures. These measures are consisting of three air variables which are air temperature, relative humidity and air velocity. Standards and codes were developed and had defined limitation as requirements to be used in determining calculated thermal loads for buildings. Design and implementation of these measures have not shown to assess the thermal comfort sensation to people in various applications. Experiments were run to capture air variable conditions in actual site operation for suggesting modification and solution to HVAC industry[1]. On the other hand, computer aided design (CAD) and simulation techniques have interfered in HVAC industry efficiently where studies were conducted towards types of air flow distribution. Various means of air supply such as side wall,

ceiling and under floor types has proved to be factor in affecting air flow distribution. Ceiling supply inlets has shown to be a good choice for dense occupied spaces. In addition, types of AC system utilized in the space showed to affect the relative humidity for the time it consumes to reduce humidity. However, changing AC system and air outlets type has shown to highly improve thermal comfort measures as it is mainly depending on physiology of human body in addition to indoor and outdoor conditions[2–4]. CFD tool is used recently in determining the best model could be achieved for air flow distribution and energy demand in air conditioning application. Even though, simulating air variable via CFD and finite volume methods have not shown to describe and present the thermal comfort to humans. Thermal comfort indices (PMV and PPD) were described and implemented in a model prepared by Fanger[5]. Thermal comfort was analyzed for several applications such as offices, air craft cabins, metro station and etc. via Franger's model in addition to air variable (air temperature, air velocity and relative humidity) which was studied to show more detailed analysis[6,7]. Indraganti and Boussa [8] have obtained thermal comfort measures at 24 ℃ air temperature for ten office buildings located in Doha, Qatar. Another study was conducted for the air temperature metro hall station where the average air temperature was found to be 27 ℃[9]. Other application like air craft cabin showed no air drafts in the studied air flow distribution and PMV and PPD was calculated to be 0.2 (neutral) and 15% (dissatisfied occupants) respectively[10]. Other studies showed air temperature and relative humidity in range of 24-28 ℃ and 50-55% respectively. [8-10]

1.2 Thesis motivation

Major function of air conditioning system is to provide indoor condition for people to do their usual practice in uniform manner. It is a role to control humidity and air

temperature by increasing or decreasing it in line with humidification and dehumidification process. It becomes challengeable in some applications such as swimming pool due to high air moisture content which is induced mainly from pool water evaporation. Controlling air temperature, air velocity and relative humidity can be accomplished through normal operation of AC system in most of applications where there is no precise control of humidity. However, it does require to capture and tackle moisture distribution during the operation of swimming pool as pool basin is subjected evaporation process all round year. This topic is considered to be one of the most researchable areas in HVAC industry due to the complexity of modeling evaporation behavior in line with air variables and thermal comfort indices. Even though, studies are shown to be minor in swimming pool applications. Few researches were prepared on studying thermal comfort and air flow variables in Indoor swimming pools. In addition, no studies have been carried for studying indoor environment and thermal comfort for swimming pools in the middle east region. Thus, it adds novelty to this area of study to investigate thermal comfort and air flow variable for indoor swimming pool in hot and arid regions. Evaporation of water from pool basin and indoor conditions control are the key factors and difficulties in studying this topic considering sever outdoor conditions for hot countries.

1.3 Thesis objective

Few studies have been conducted on air variable in Europe regions, investigating air flow variable distributions (air temperature, relative humidity and air velocities). Moreover, verification of boundary conditions was not shown for most of the studies obtained as part from showing that optimum results of indoor conditions are achieved or not. Especially, air flow rate which was defined by ASHRAE that it should be between 4 – 6 ACH (Air Change per Hour) in indoor swimming pools for good indoor

air quality. In addition to that evaporation phenomenon and humidity issues were not elaborated and discussed in details which is considered as main factor in deteriorating interiors of building as highlighted in ASHRAE standards chapter 6 indoor swimming pools. Studies showed to use air variables in assessing thermal comfort which is considered to be following the recommended limits of ASHRAE standards instead of Franger's Model. Moreover, incorporating all these weak points in a study of indoor swimming pool located in Doha, Qatar makes its more interesting towards possible findings that could be achieved.

This can be achieved through the following objectives:

1- Study all recent investigations for applications including humidity control and indoor conditions issues.
2- Obtain a physical model from literature and validate it for this thermal study.
3- Compute cooling load calculations, evaporation rate from pool basin and verify all the boundary conditions used from the calculation.
4- Use CFD modelling in capturing the air flow distribution and all air variables (air temperature, air velocity and relative humidity) for winter and summer seasons.
5- Conduct thermal comfort analysis using PMV and PPD indices for winter and summer scenarios.

1.4 Thesis Outline

The breakdown of the thesis chapters is presented as follows:

Chapter 1 general overview of the topic is briefly introduced along with thesis motivation, outline and objectives.

Chapter 2 detailed literature review is presented on indoor air flow study for green houses through various cooling approaches and combination of them. In addition, to that thermal comfort, air flow parameters(variables) and indoor air quality are showed

under the literature review of indoor swimming pools.

Chapter 3 Methods used in carrying this study are described in details. Firstly, physical model was prepared using CAD software (Solidworks). Then inputs, criteria of cooling load calculation, evaporation rate of pool water were discussed as per ASHRAE standard and Qatar local authority regulations. Theory of Finite volume method and CFD model were detailed including numerical grid formation.

Chapter 4 illustrates manual cooling load calculation and results of validation work to show the applicability of using the model of Ciuman et al. [41]. Moreover, Results of cooling load by HAP were verified using ACH verification method as defined by ASHRAE standards. Boundary conditions were derived from cooling load calculation output and used in obtaining numerical results of Qatar model. Then, contours plot of air temperature, relative humidity and air velocity were presented and discussed for both summer and winter seasons. Finally, thermal comfort indices were computed using Franger's model and results of PMV, PPD and air variables were summarized for each seasonal scenario.

Chapter 5 in this chapter, listing all obtained results and showing their verification with recommended values in standards and regulations. Moreover, conclusion showed all points of comparison between thesis findings and other findings using average of each air variable. Using thermal comfort analysis to assess thermal comfort in more detail studies. In addition, recommended improvements and gap of knowledge are discussed be considered in future work. Including energy analysis and experimental work as new area of research in the thermal study of indoor swimming pools in hot and arid environment.

CHAPTER 2. LITERATURE REVIEW

In this chapter, an Extensive literature review has been conducted for high humid applications such as green houses and indoor swimming pools. In the first part, various cooling system types were applied to achieve the optimum indoor conditions in green houses and the results were obtained using both CFD modelling and experimental work. Some of these researches were carried for Qatar; however, they are not intended for testing indoor environment and thermal comfort in indoor swimming pool in Qatar. The second part of this study will be discussing the finding of thermal comfort and indoor quality for indoor swimming pools. Lack of studies was expressed in few researches carried for indoor swimming pools and especially for hot arid and humid regions in the middle east such as Qatar.

2.1 CFD Modelling for green houses

2.1.1 Evaporative cooling

A validation for thermal performance was carried on evaporative cooling greenhouse type located in Alkhor, Qatar. Ghani *et al.* [11] used CFD simulation to validate the results of global incident solar radiation, air temperature, and relative humidity with the measured data for 1000 m^2 greenhouse area. The standard K-□ model, which is suitable for the considered modeling cases in this thesis [12] was used for a computational domain of 4,500,000 tetrahedral elements. Temperature comparison showed 4℃ difference at three different elevations on the greenhouse. 2% absolute error was determined for relative humidity at the same elevation used for temperature verification. The outside and inside solar radiation has shown an average error of 5.3% - 5.6% between measured and validated results. Another parameter such as ventilation rates showed inverse proportionality with temperature. It was proved by this study that as ventilation rates increase for values higher than 60 ACH, temperature gradients

decrease inside the greenhouse [12].

Xu *et al.* [13] developed experiment for testing evaporative cooling pad systems in a glass span warehouse, 2304 m^2 in shanghai, China. The relative humidity and temperature distribution were measured using humidity probes and thermistor thermometer respectively. Evaporative cooling method utilized with other methods such as external shading, inside thermal screens, and circular fans to reach the optimum cooling performance. Outdoor Incident Solar radiation and high relative humidity values has shown high energy requirement to overcome. The outdoor temperature was cooled down to 28 ℃ at the condition of relative humidity 70%. In addition to that the humidity ratio has increased the condition from 0.0202 to 0.0236 kg/kg dry air to obtain the indoor condition requirement. Introducing external shading and thermal screens option with evaporative cooling has reduced more the indoor temperature 6 to 7 ℃ [14] Circular fans were adopted in line with these methods to ensure that there is no any air stratification area as shown in (Fig. 1). The effect of addition of circular fans has improved the temperature distribution specially at height of 4 m from the ground level. In other words, the hot air was stilled at high levels of the greenhouse due to buoyancy effect. As a summary of these results indoor air temperature can be kept between 2-3℃ under RH 80% through using evaporative cooling and shading methods.

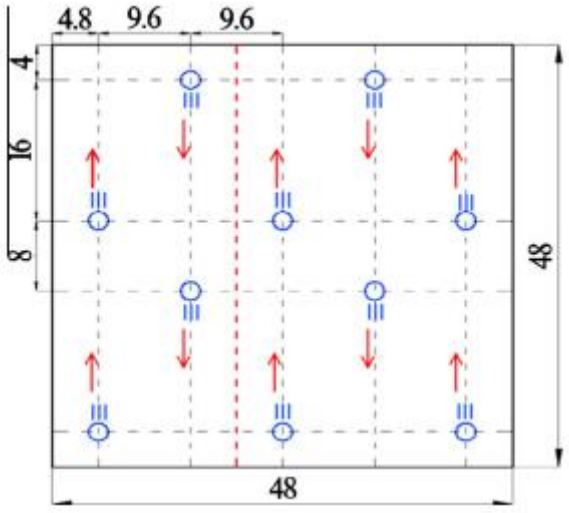

Figure 1. circular fans distribution layout showing the location of fans in the greenhouse. [14]

Research was conducted by Lertsatitthanakorn et al. [15]for utilizing direct evaporative cooling in silkworm production house of 32 m^2. The silkworm house was built and tested in Mahasarakham University, Thailand [16]. A cooling pad (1.8m x 3.6m) with fan was installed on north and south walls. The experiment was performed in tow duration: November-December 2003 and March-April 2004 using Testo model 175-H2 as a measuring instrument for temperature and humidity. The objective of this study was to test the performance of air-condition system at on-odd mode under certain conditions. For cooling system - Off condition, the room has reached the ambient temperature at 14:00 due to the infiltration of air through the cooling pads. Then the indoor air temperature was increased to reach a maximum value of 33.1℃ because of the heat contaminated inside the room. On the other hand, the room temperature was reduced to 22.1 ℃ and relative humidity increased from 33% to 82% in the on condition of cooling system. It was found that the temperature decreased from 39.2 ℃ to 26.1 ℃ and relative humidity (RH) increased to 51.2% in summer season. The RH was found to be high in winter compared to summer season due to the lower temperature drop

(10.1℃) encountered in winter season. This variation in RH levels indicates high moisture content in winter against summer season. The third part of this research was to obtain the cooling effect in line with varying airflow rates for 4.4, 6.3 and 9.2 kg/s. It was clearly found that the temperature is reduced as air mass flow rates increased in contrast with RH that has showed no effect as air flow rates increased. Applying direct evaporative cooling to silk room production house has proven its effectivity in achieving the required indoor condition of low air temperature and high relative humidity.

A study was conducted by Kittas et al. [17] on the indoor environment response for a greenhouse using evaporative cooling pad and screen house. The experiment was prepared in Sultan Qaboos University in Oman for winter-spring and spring-summer seasons. Tow 180 m^2 tunnel shape greenhouse was built one covered by polyethylene and the other covered by screen. Indoor air temperature and relative humidity measurements was obtained by HT-732-H-26 temperature sensor and HMP45C humidity sensor respectively. Incident solar radiation was measured from February to May as 12 to 33 Mj/m^2 and wind speed with maximum value of 6 to 5 m/s for the same duration. The mean temperature was measured to be 25.9 ℃, 31.8 ℃ and 30.5 ℃ for greenhouse, screenhouse and outdoor environment respectively. This indicates that the outdoor temperature is lower than the indoor temperature for screenhouse by 1.3℃ and higher than indoor temperature for greenhouse by 4.4℃. Moreover, it was expected to found no temperature difference as the air supplied is not forced into the space. In addition to that other researcher achieved the same temperature gradients using evaporative pad-fan cooling system [18–20]. Screenhouse shown its disability to overcome the accumulation of heat internally without any cooling equipment. In contrast Leyva et al. and Sonneveld et al [21,22] used fog system inside the screenhouse

using to improve the indoor environment conditions. The RH has shown to increase by 20% RH with negligible effect on air temperature. In contrast, air temperature is reduced via utilizing free-moving shading or (near infrared radiation reflective materials in the screenhouse. In addition to a 50% reduction in solar radiation was achieved which indeed reduced the solar radiation heat load.

2.1.2 Fog cooling system

Almulla et al. [23,24] and Perdigonesa et al. [25] applied fog cooling system with other combination of cooling techniques in studying the temperature difference between indoor and ambient environment for greenhouse of 132 m^2. The studied green house is located in Madrid, Spain and constructed of steel frame with a one layer of methacrylate cover. The first part of this research was conducting analysis on the variance of climatic parameters. The analysis obtained no temperature difference between indoor and outdoor. The results achieved were obtained by various techniques like shaded screen, fogged above screen and fogged under screen. A dynamic model was prepared using energy balance to validate the experimental work. The dynamic model showed small error for an indoor temperature difference lower than 1.5 °C with experimental work. The last part was the numerical analysis validation which had shown a variation in the temperature difference at 5% error. This can be interpreted as fogging frequency decreases; temperature gap will increase for the technique of fogging above shade. Combining shade screen with ventilation showed optimum reductions in temperature and producing low relative humidity levels. The novel outcome of this research was found for mean indoor temperature (22.9 °C) and maximum indoor temperature (28.9 °C) at fogging rate of 6.1 lm^{-2}/day for fogging under-screen technique. In contrast, cooling effect is not enhanced for no shade technique due to high amount of radiation enters the greenhouse area but the RH levels has decreased air gets dried [26].

2.1.3 Combination of Fog and other cooling systems

CFD simulation was prepared to validate experimental work relative humidity distribution. The case study was studied on two cooling systems for a greenhouse which are fog system and dehumidifier with fog system. Fog cooling system is used for humidifying the space while dehumidifier was added in the second experiment to dehumidify the area [27]. The model was designed using GAMBIT 1.3 and ANSYS Fluent 5.3 for carrying the numerical analysis. The Physical model is located in Ansung in Republic of Korea with dimension of L: 18m, W: 6.5m and H: 2.4m. Realizable K- model was used as the turbulence model with Boussinesq model for studying natural convection, DO radiation model was used for solving radiation equations and discrete phase model for capturing the changes in environment due to spraying water into air [28,29]. Independent study was done for grids inside the greenhouse in order to ensure the accuracy of the results. The domain was divided into three zones (lower, intermediate, and higher) to clear validate accurately the experimental measurements. In the case of operating fog system, air speed was similar for both the measured and simulated value. Moreover, it was found that the absolute error for simulated relative humidity is higher than experimental results by 8.9% for lower zone, 2.8% for intermediate zone and 2.6% for higher zone. The second case was applying dehumidification process on the space using fog system with dehumidifier. Larger variation for RH contours lines was obtained due to the addition of dehumidifier to the CFD model (Fig. 2). In other words, adding the dehumidifier shoed to reduce the RH values. The fluctuated RH distribution was found to have range from 1.1 to 13% absolute error between simulated results and experimental measurements. In terms of zone comparison, experimental measurements were lower than simulated results by 3%

for lower zone, 6% for intermediate and higher zones respectively[30].

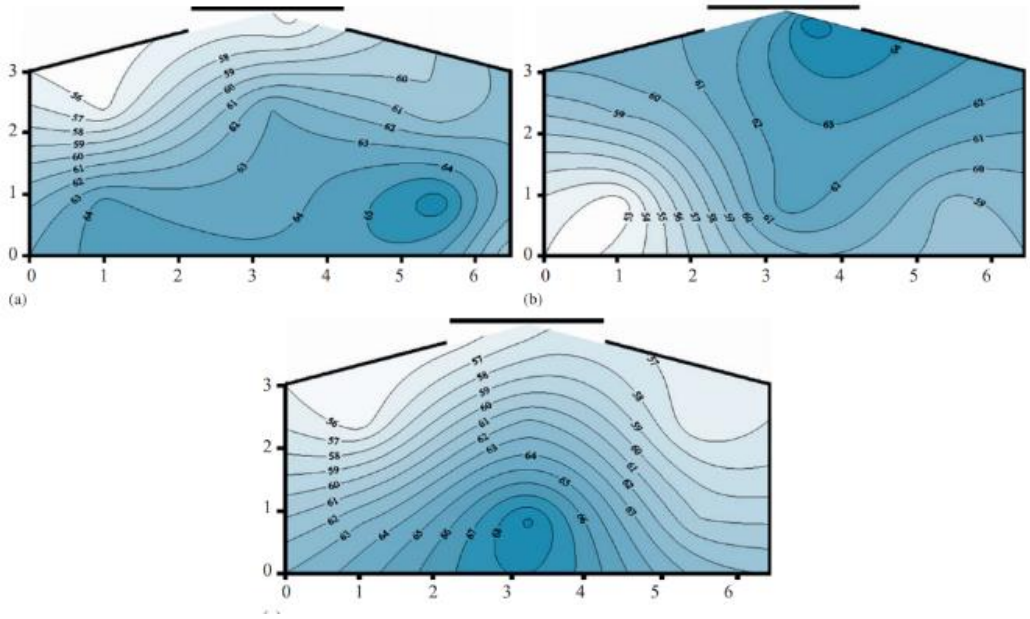

Figure 2. Relative humidity distribution with a fog cooling system and dehumidifiers (humidification plus dehumidification). [30]

Research was carried by Ishii et al. [31] for studying the indoor airflow parameters using a combination of natural ventilation and fog cooling method and comparing it with natural ventilation. Experimental work was conducted in period from June 22 and 24, 2004 Moreover, green house site (417.6 m^2) is located in Tsukuba Ibaraki, Japan. Solar radiation was measured by with pyranometer, temperature was tracked by thermocouples (copper-constantan thermocouple) and ventilation rate measurement was prepared based on 5 ppm (constant gas concentration). In duration from 10 am to 14 pm, the temperature, solar radiation and humidity was measured to be 30.9°C, 796 W/m^2 and 57.2% RH respectively. In addition to the wind speed which was measured to 2.1 m/s from the south-southwesterly. Using natural ventilation (NV) in cooling, reduced the air temperature difference between outdoor and indoor by 3.4 °C while the air flow rate was increased from 2.8 to 4.4 m^3/m^2s. The same observation

was found by using fog system with NV. Which showed 2.8 °C reduction in temperature at high airflow rates from 2 to 2.6 m^3/m^2s. Adding fog system to the natural ventilation system proven that the indoor temperature sharply reduced while relative humidity sharply raised. These can be derived from the transfer of sensible load to latent load as water is evaporated from fog into the air. The overall outcome that temperature was maintained within 26-32°C and RH for 60 to 100% through using the combination of natural ventilation and fog system compared natural ventilation[32].

2.2 CFD Modelling for swimming pool

2.2.1Thermal Comfort

A study carried for thermal comfort and indoor air quality (IAQ) inside swimming pool by Lebon et al. [33] A numerical code was prepared for an indoor swimming pool located in "Bishop's University (Sherbrooke, Quebec, Canada)" using TRNSYS software (version 17) [34]. The developed numerical code is based on zonal method which had divided the calculation domain into 38 zones. Thus, it will be able to investigate the heat transfer and mass transfer process between water surface and air. The Matlab code used airflow rates as an input to compute the temperature as a result for each zone at a time step of 15 minute and convergence criteria of 10^{-4} (nearly1000 iterations). The boundary conditions were defined at the water surface for a temperature and relative humidity (RH) of 29 °C and 100 % respectively. Furthermore, 20 air flow inlets were assigned with 918.75 kg/h each, air temperature of 35 °C and RH of 55 %. The regional data integrated with TRNSYS software was used to define the Solar radiation and Outdoor conditions. Furthermore, lighting fixtures were treated as warm surface with Lighting Power Density (LPD) of 2 w/m^2. Zero heat gains were assigned to people by assuming the building is not occupied. The computed results were validated by air temperature, relative humidity, and velocity measurements. The

temperature has shown a linear relationship with height for supply air temperature of 35 °C. An average of 3 °C temperature difference was obtained between the calculated and measured temperature for all heights. Moreover, the temperature difference was reduced to 2 °C in areas near to ground level and 2.5 °C difference for ceiling temperature. The calculated and measured values for relative humidity have shown good agreement with 5% absolute error where it increased in regions near water surface. In addition, it was found that computed relative humidity has exceeded the recommended range (50-60%) by ASHRAE standards. Some areas have shown 30% absolute error between the calculated and measured values due to using measuring devices in improper location. Thus, the measuring accuracy of device decreased with long distance of measuring. On the other hand, the standard deviation was calculated 0.05 m/s for a range of 0.1 to 0.35 m/s air speed which still in the range of recommended air velocities by ASHRAE standard. The second part of this study was to evaluate the indoor air quality and thermal comfort indices (PMV-PPD), 6-8 ACH (IAQ) was obtained for 31 to 36 zone out of 38 zones. The obtained range of IAQ has showed to be in the range of Indoor air quality ranges (4-8 ACH) by ASHRAE standards. Moreover, all zones showed acceptable ranges for thermal comfort except six zones. These six zones have shown Predicated Mean Vote (PMV) values higher than +1. PMV values of range between -0.5 and +0.5 have been achieved by two zones. On the other hand, the dissatisfaction using Predicated Percentage of Dissatisfied (PPD) was obtained for six zones (zone 8, 19,21, 32, 33, and 20) and only zone 7 has achieved stratification.

Limane et al. [35,36] used OpenFOAM software to study the air variables for semi-Olympic pool in Bishop's University in Sherbrooke (Quebec, Canada) as shown in (Fig. 3). CFD simulation results were compared with measurements taken for temperature,

air velocity and humidity. Numerical calculations were computed for Summer and winter seasons. K-□ standard model was used as the turbulence model while sharma and launder model was used as evaporation models. Air was delivered at a velocity of 3.5 m/s and temperature of 35 °C and humidity of 45%. The water temperature was assigned with a temperature of 29 °C and relative humidity of 100%. Moreover, the domain was meshed in hexahedron mesh type with fine resolution. The number of cells was obtained 26,921,201 cells as a result of the meshing process. Velocity profiles showed high velocity rates concentrated at the air outlets. On the other hand, low velocity regions were determined near the occupant's sitting area. In addition to that, recirculation zones were obtained at some areas and this has showed discomfort to occupants. In contrast, return air recirculates its path for areas near false ceiling in the winter season. Moreover, it was observed that fresh intake air reaches the occupant area faster in summer compared to winter. Temperature profiles has shown to follow the same profile of fresh intake air in summer and winter season. 3 °C temperature difference was obtained between measured and numerical results. Furthermore, high humid areas were observed near the basin surface and low relative humidity near the air outlets as shown in (Fig. 4). Humid areas are clearly shown in relative humidity contours where the RH ranged from 50-60% at spectator areas. The second part of this study was to investigate the effect of swimmers on air flow pattern. The air velocity was found to be reach a maximum value of 1 m/s above the water surface. The air velocity results were found to be similar for both swimmers and non-swimmers in winter season and vice versa for summer season. The existence of swimmers forced air to flow from air outlet towards the diving board. It can be noted from the air velocities contours that flow of air tends to increase in the cold areas at the presence of swimmers. To conclude, air stratification and thermal discomfort were presented in the air variable

profiles due to the geometry of swimming pool, poor recirculation of air and the accumulation of hot and cold layers.

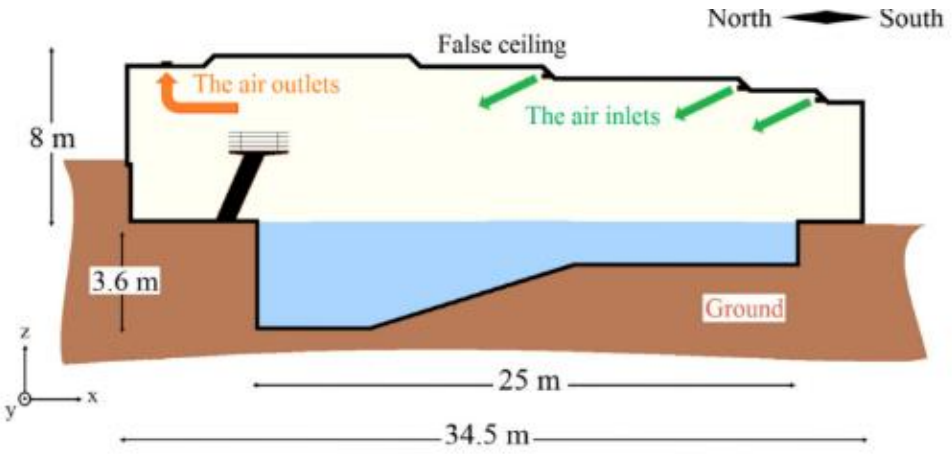

Figure 3. Sectional view of semi-Olympic pool in Bishop's University in Sherbrooke (Quebec, Canada)[35].

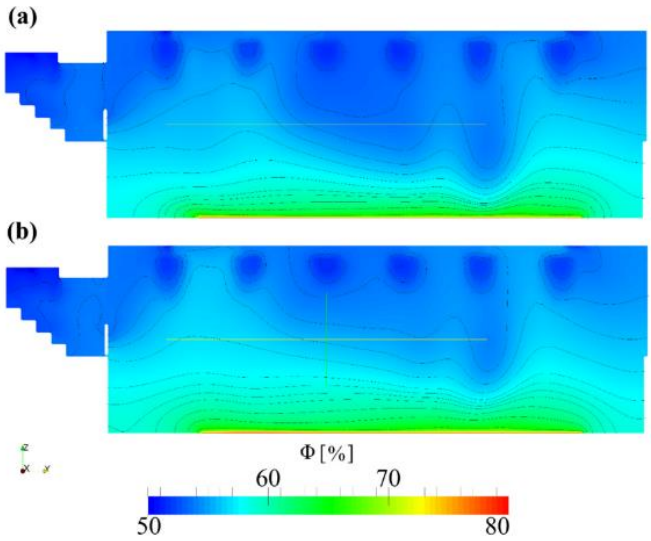

Figure 4. Relative Humidity Contours obtained for sectional view of semi-Olympic pool in Bishop's University[36].

2.2.2 Indoor Air Quality

Addas et al. [37] studied the thermal comfort and Indoor air quality for Afjord swimming pool in Norway. Tow parameters were tested for Indoor air quality which

are local mean age of air (LMA) and air exchange efficiency indicator (ACE). A CFD model was prepared using Star CCM+ software to investigate various ventilation methods effect such as MV (3.5 ACH), MV-DV(5.5 ACH) and DV(4,5,7 ACH). A polyhedral mesh with prism layer was utilized in the preprocessing phase and the result was 420,000 cells. Furthermore, Standard K-w model was used as the turbulence model but, chlorine with water vapor and air as studied using species transport species [38]. In addition to the radiation effect applied to the space was studied by surface-to-surface radiation model. Shah model was incorporated to represent the evaporation rate from water surface. DV 7 was used as a reference for measuring the chlorine concentration reduction against the other ventilation methods. DV 4 and DV 5 have shown to increase the chlorine concentration by 1 and 0.5% respectively in the breathing zone. In contrast, MV-DV and DV reduced the concentration of chlorine by 36 and 21% respectively. The breathing zone was defined in this study as the zone covered by air flow at a distance of 1.6 m from the floor surface and 10 cm above water surface. LMA has increased in the unoccupied zones while it was decreased for bath area using MV-DV and DV systems. In contrast ACE showed high values for MV compared to MV-DV which means that MV-DV is using more energy compared to MV method. Moreover, the draught risk behavior was observed to occur in MV system. Moreover, it was obtained that the thermal comfort was achieved at an average air velocity of 0.4 m/s using MV system. The relative humidity values decreased for MV-DV system (50-58% RH) compared to DV system (60% RH). These all observations indicate that no stagnant air areas were observed and no condensation were found on the internal structure of the space.

2.2.3 Air flow Parameters

2D and 3D CFD simulation studies were done on a swimming pool in Korsor

Svommehal (Denmark). Evaporation rate as computed and used int the study for occupied and unoccupied swimming pool case. Numerical calculation was computed in fluent 6.1.18 at steady state conditions with boundary conditions of air temperature, relative humidity, water temperature and air velocity. Standard K-□ model was used with species transport model to describe the turbulence behavior inside the pool. It was concluded that the RH was highly affect in the 2d simulation due to the evaporation rate from water surface. The convergence criteria were specified as 0.0001 with 8,500 grids for the 2D simulation case. On the other hand, the 3d simulation was prepared on convergence criterion of 0.001 and 645,408 grids. Results of air temperature and air velocity were found to be similar for both occupied and unoccupied scenarios. The scientific investigation for this similarity is highlighted in the small amount of mass fraction of water vapor that was presented in the occupied and unoccupied cases. Moreover, relative humidity was found to be high in occupied case one due to the high evaporation rate from pool basin[39,40].

SST k-ω model was used by Ciuman et al. [41] in an indoor swimming pool located in a school in Gliwice, Poland as shown in (Fig. 5). Numerical calculations were conducted using Ansys CFX 14.5 under non isothermal and steady state conditions. Rhie-Chow algorithm and second-order upwind methods was applied in the numerical problem. Moreover, species transport model as used to present the moisture content of air in the space. The convergence was obtained at 2000 iterations at pressure and velocity residuals of 0.0005 for case 1 and 0.0003 for case 2 and 3. Meshing has been applied into 3 cases (case 1: s1, case 2: s2 & case 3: s3) for an unstructured tetrahedron element with high refinement (hexahedron elements). Refinement has been applied only to s2 and s3 grids at the boundary layer of water surface. Detailed comparison was prepared between numerical and experimental work in terms of

temperature, air velocity and relative humidity. A deviation of 0.11 m/s was obtained at height of 0.1 m for all cases. The air flow creates turbulent behavior near the walls of the swimming pool basin thus, this deviation was obtained in air velocity. Secondly, the indoor air temperature was measured as 26.3°C-27.8 °C for case 1 which varied form the simulated result by 0.1 °C. In case 2, the temperature was 0.4 °C lower than the measured temperature while air temperature was measured as 25.3°C-25.8 °C. On the other hand, air temperature was measured as 27.5°C-27.9 °C which was found to be numerically higher with 0.8 °C. In contrast, relative humidity has shown high accuracy for all cases except case 3 where the absolute error was obtained 2.2% at 0.1 m height. Contours plot of relative humidity, temperature and air velocity were obtained by the numerical analysis are shown in (Fig. 6).

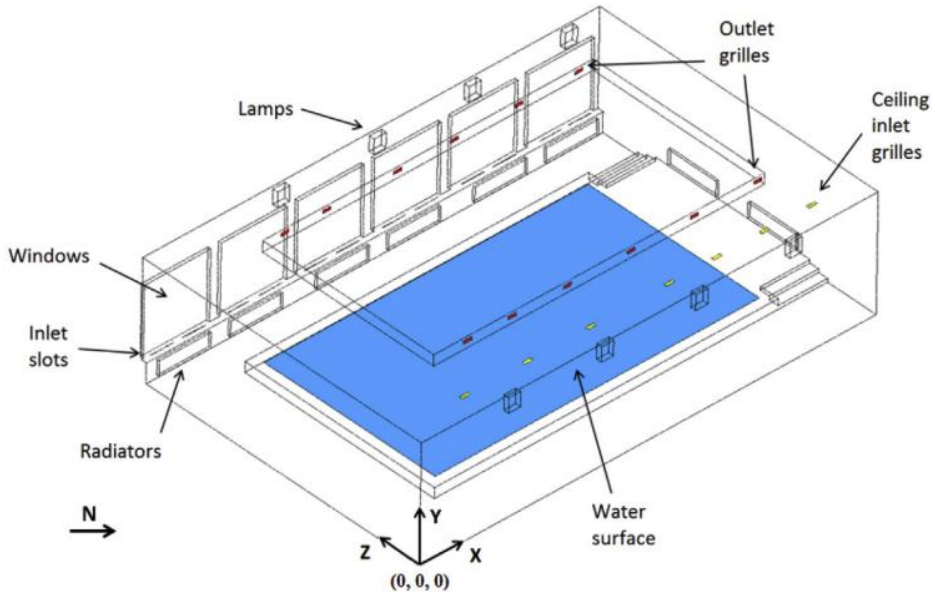

Figure 5. 3d model of indoor swimming pool located in a school in Gliwice, Poland[41].

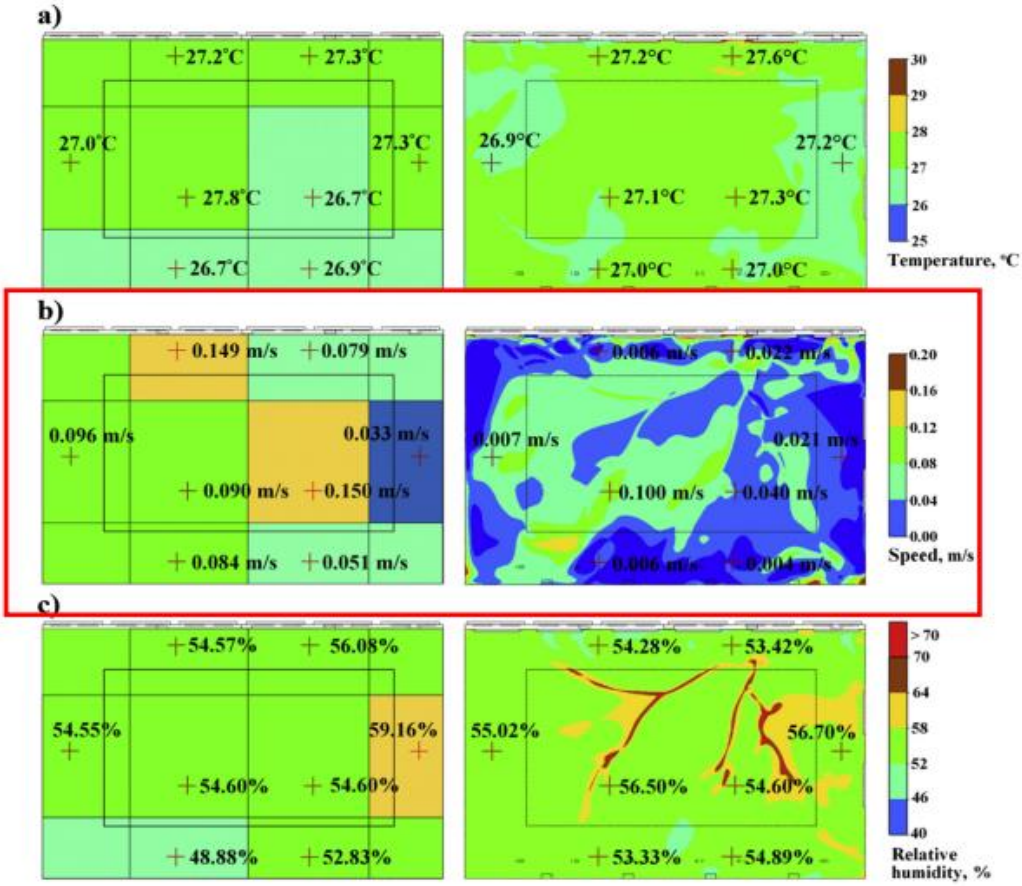

Figure 6. Contours plot for 1) indoor air temperature, 2) air velocity, 3) relative humidity at height 0.2 & 0.6 m from swimming pool basin surface[41].

Different evaporation rates were used by Elazm et al. [42] in his study to show their effect on indoor quality of a swimming pool. The simulated pool is located in San-Stefno grand plaza in Alexandria, Egypt. Relative humidity and temperature were measured at three breathing zone levels taken from pool deck which are level 1 (50 cm), level 2 (100 cm) and level 3(200 cm). Air flow was assumed to be turbulent through utilizing standard K-□ model and transport species for moisture content at steady state conditions. The 2d domain was discretized into 8500 cells at 0.000001 convergence criteria. Boundary condition was expressed in assigning walls with constant temperature of 25℃ , inlet air velocity by 1.26 m/s and supply air temperature 27℃. Simulation contours showed that air velocity tend to be maximum of 0.2 m/s at

evaporation rate of 1 kg/s and 1 m from the pool basin surface. In contrast, temperature and mass fraction of water vapor reached their maximum value at 0.5 m height with evaporation rate of 3 kg/s. It was clearly observed from this research that evaporation rate and mass fraction of water vapor are directly proportional. In addition to that inverse relation was obtained by RH and air temperature reduction when the air velocity as increased. As a result, the increase obtained in the evaporation rate is derived from the low temperature difference created between water surface and indoor air.

A competition swimming pool located in "Città dello Sport" in Rome was studied numerically for air velocity and temperature. The pool was designed to host world swimming championships. Moreover, it was clearly highlighted by the author that peak thermal loads were estimated improperly for many reasons such as the complexity of the structure design, solar radiation effect, heat dissipated from electrical items and occupant loads. In this study the fluid was treated as incompressible inside a domain of 200 faces and 880000 cells. Tetrahedral and triangular meshing was applied to cells and faces respectively. Two scenarios of CFD simulation were studied at winter season (HVAC system is off) and summer season (HVAC system is in operation). In winter season, results showed that the hot air was accumulated as layers upstream the spectators with an average velocity of 0.3 m/s and average temperature of 15 ℃ at 50 cm height in the occupied zone. Operating the heating ventilation and air conditioning (HVAC) system during summer season showed higher velocities in the occupied zone with air speeds and temperature higher than 0.4 m/s and 29 ℃ respectively. The outcome of two studied seasons that HVAC system has control in winter season humidity. It can be achieved by modulating the direction of nozzles and their air flow rates. On the other hand, it was clearly considered in his recommendation for this study that studying and obtaining good estimations for lighting, solar radiation, and occupant

load are mandatory during summer season. Therefore, it was recommended by the researcher to keep the air temperature in range of 26-29 ℃ during normal operation and 28 ℃ during competitions to achieve thermal comfort as recommended in ASHRAE standards [43].

CHAPTER 3: METHODOLOGY

The study was conducted using a variety of tools, techniques, and technical knowledge, which are included in these four sections as the following: geometry modeling, thermal loads, CFD simulations, and thermal comfort indices. This thesis' physical model was created using CAD software (Solidworks). Then, thermal load calculations were performed using energy modeling software (HAP Carrier), with all necessary inputs coming directly from the study's geometry. According to section 3.2, the necessary input parameters were chosen for the conditions in Qatar. The results of the cooling load calculation were used to execute the CFD simulation, and an independent grid study was created to verify the chosen grid element count. Additionally, Section 3.3 covered boundary conditions, moisture models, and turbulence models, outlining all techniques for doing the numerical analysis. Last but not least, the results of the CFD simulation were used to analyze the thermal comfort experience for humans using Fanger's model. Fanger's model's input variables are all explained in section 3.4.

3.1 Geometry modelling

Swimming pool has a dimension of 17.6 x 11.7 x 4.4 m (L x W x H) which was built using Solidworks CAD software. The pool basin was designed in a regular rectangle shape of (12.5 x 7 x 1.36 m) as shown in (Fig. 7a). For the purposes of this new study, all variables were employed as reported in [41] with the exception of location, which was changed to Qatar. A perimeter wall standing 40 cm above the ground encircled the pool basin. Internally, walls were treated as internal partitions, only two outdoor walls—those facing north west (NW) and south west (SW) were exposed to the outside environment. On the SW exposed wall side, six windows (each measuring 2.5 x 2.5 m)

were added. Four 250-watt bulbs are mounted in the SW direction on the high wall above the windows. Six radiators were also installed below the window on the low wall side. Other Two more radiators were fixed, orienting toward the northwest. It was installed in the space as Europe region use heating system instead of cooling system. Therefore, it will be excluded form the analysis in this study. Ceiling intake grills (0.28 x 0.0975 m) supplied air in the direction of north-east (NE) side. Inlet slots (0.87 x 0.019 m), which were situated below window used to supply air parallel to the window glazing, as second method of air supplying. While return air is exhausted horizontally through outlet grills with a diameter of 0.28 x 0.0975 m that are situated in the centre of the drop-down ceiling. All swimming pool fixture and component can be clearly seen in model (Fig. 7b).

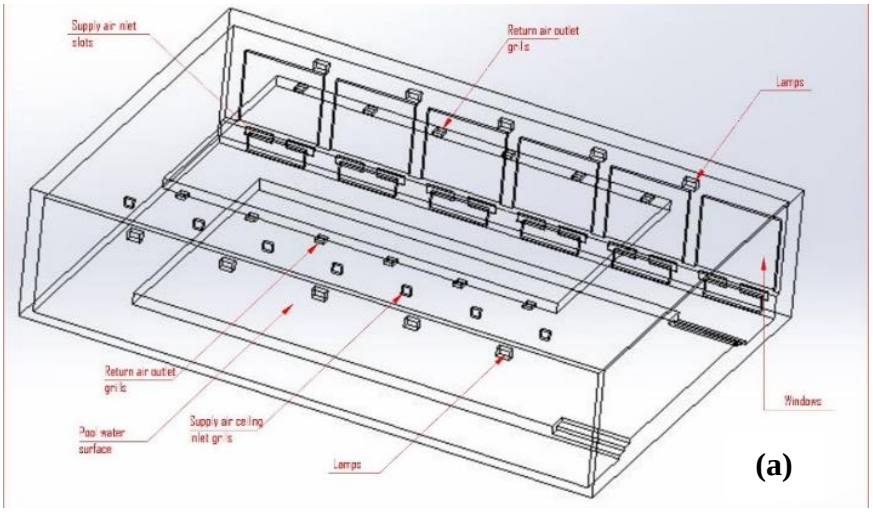

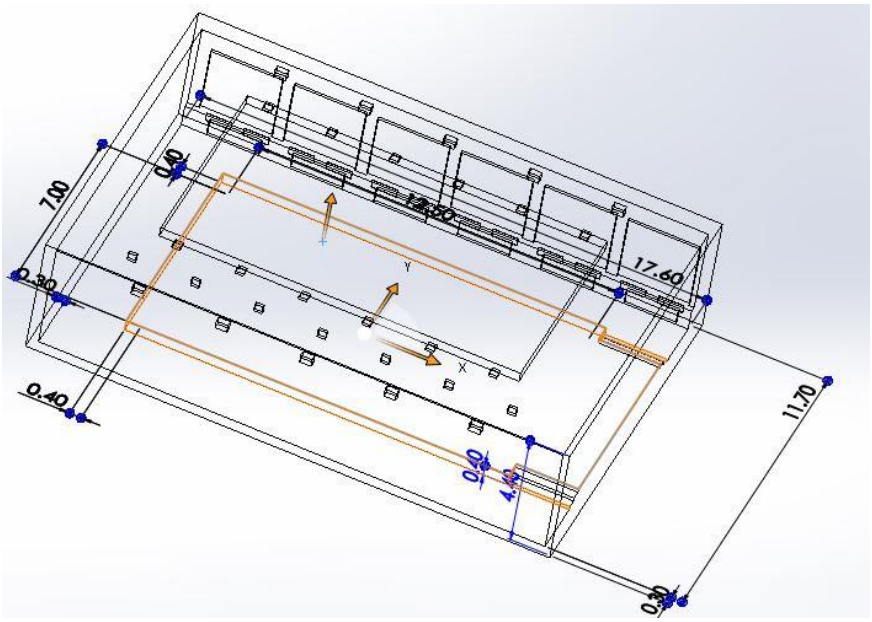

Figure 7. 3d Solid works model of the indoor swimming pool (a) Detailed dimension model (b) Internal fixtures.

3.2 Thermal loads

Swimming pools are thought to be a challenging application in regulating **(b)** ty and indoor air temperature. In the middle east's arid and humid regions like Qatar, it is more difficult to study it. With the following external conditions of 43.3 °C dry-bulb temperature (DBT), 33.3 °C wet-bulb temperature (WBT) in the summer and 17 °C DBT, 8.6 °C WBT in the winter, cooling impact also becomes a significant factor in HVAC application for this space[44]. The estimated thermal loads in the pool were calculated using the HAP 4.9 (Hourly Analysis Program) cooling load calculation program. According to the 9th edition of the ASHRAE Pocket Guide, thermal loads are classified as internal, external, and infiltration [44,45]. External loads are heat transfer occurred between outdoor environment and any structural element, including the roof, walls, glass, ceiling, and interior partitions. According to Kharama Conservation Code

(Kharama: Qatar General Electricity and Water Corporation) and Qatar Construction Standard (QCS), U-values were used in calculating external loads. On the other hand, internal loads are heat dissipated from people, lighting, equipment, and appliances inside the space. Lamps (lighting) and radiators (equipment) are added as indirect internal loads. Infiltration load was neglected as it was not increasing the thermal load. The facility was planned to be open for 10 hours every day from 8 AM to 6 PM from September to June. The occupant load (number of people) is calculated using the occupant density from table 6-1 of ASHRAE standard 62.1[46]. It was determined that 7 people could occupy in the area using the play area category with occupant density of 0.07 m2/person. Because it significantly increases the total thermal load and humidity in the swimming pool, the latent load of the pool basin was regarded as essential factor in achieving indoor design condition and thereby thermal comfort. Pool water evaporation caused this latent load as a result of the temperature difference between water's surface and indoor air. According to Smith et al. (1993) and the ASHRAE application guide, the evaporation rate was calculated as 0.005565 kg/s (13.541 kw) using (Eq. 1) [47]. Then it was added as latent load in the total cooling load calculation. The Total cooling load 61.9 kW (17.6 TR) were calculated using HAP space input is discussed in Table 1. In HAP system output, AHU (Air Handling Unit) has been defined as the air conditioning system with indoor conditions of 23.5 °C and 50% RH as recommended by ASHRAE standards. Moreover, the supply air temperature of air outlets used to encounter the required indoor environment condition was set to 19.8 °C.

$$w_P = 4 \text{ x } 10^{-5} A(p_w - p_a)F_a \quad (1)$$

w_P is evaporation of water [kg/s]

A is area of pool surface $[m^2]$

F_a is activity factor (Level of occupant activity)

p_w is saturation vapor pressure at surface water temprature, [kPa]

p_a is saturation pressure at room air dew point, [kPa]

Table 1 HAP cooling load calculation inputs

Parameter	value	reference
Occupant load	14 persons	Table 6-1, ASHRAE standard 62.1 (category: play area) [45]
Miscellaneous loads	Latent load: 13541 watts 46204 btu/hr	Natatorium, ASHRAE applications handbook 2019 (Eq.1) [46]
Lighting power density (LPD)	4.7 W/m^2 0.44 W/ft^2	Table 2 Lighting power densities table using space by space method, ASHRAE fundamentals handbook[47]
External Wall U-value	0.536 W/m^2℃ 0.100 btu/hr/ft^2°F	Kharama energy and water conservation code
Roof U-value	0.437 W/m^2℃ 0.077 btu/hr/ft^2°F	Kharama energy and water conservation code
Glazing U-value	2.1 W/m^2℃	Qatar Construction Standards (QCS)
Shading Coefficient (SC)	0.370 btu/hr/ft^2°F SC=0.4	
Outdoor conditions (Summer/Winter)	43.3℃ (109.4°F)DBT 33.3℃ (91.94°F)WBT / 17 ℃(62.6°F)DBT 10.6℃(51.08°F)WBT	(Sleiti et al., 2022) [44]

3.3 CFD Simulation

CFD is a method for studying heat transfer, chemical reactions, and fluid flow problems in fluid systems. It examines the fluid flow pattern characteristics solving the mathematical equations that govern fluid flow systems using CFD Codes[48]. The production and research development of jet engines uses CFD techniques in the improvements of engines in the aerospace sector. Additionally, it was applied to the creation of combustion chambers for internal combustion engines and gas turbines.

Industries involved in fluid dynamics have expressed interest in the CFD tool for a variety of reasons, including the fact that it efficiently reduces design time and cost, studies for complex situations, and offers a limitless number of solutions and outcomes. Successful CFD operation requires a skilled operator [49,50]. Solution is computed iteratively within convergence criteria defined by user called residuals. To obtain high convergence, controlling residuals necessitates manipulating relaxation variables for which there are no applied standard values. Grids and cells are used to partition the domain of any fluid problem. Nodes, which indicate the resolution of any fluid flow, are included within cells. The estimation of the solution is better the more cells that were computed. The grid's internal shape is specified using finite volume discretization. For 1D and 2D simulation, quadrilateral and triangular grids are the most common grid shapes. Hexahedral, prismatic, and tetrahedral are the shapes used in 3D simulation type and considered as unstructured grid types. The discrete equation is derived by integrating the conservation equation across the control volume for each cell, as illustrated in (Fig. 8). In any CFD simulation, the approach employed by the CFD solver is represented as a set of governing equations. The three governing equations—continuity (Eq. 2), energy (Eq. 3) and Navier-Stokes equations (Eq. 4)—are utilized to solve for 2D and 3D simulations in addition to (Eq. 5) for th

e K-□ model [51,52].

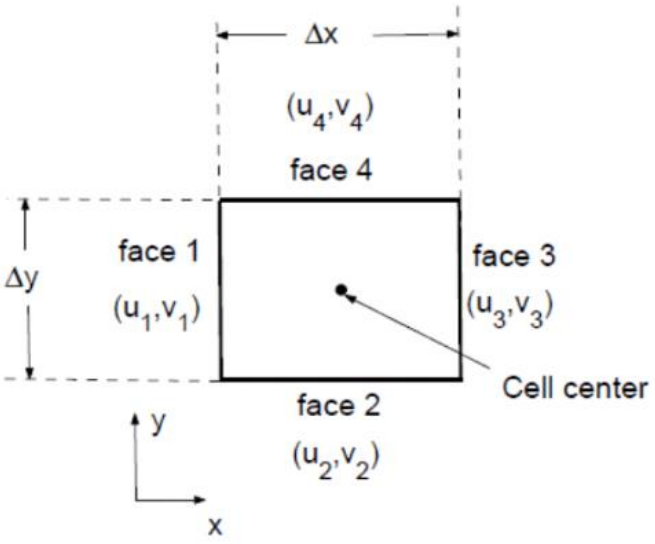

Figure 8. control volume of each cell in the domain[52].

$$\frac{\partial \rho}{\partial t} + \frac{\partial}{\partial x_i}(\rho U_i) = 0 \qquad (2)$$

ρ is density of the fluid [kg/m^3]

t is time [s]

U_i is mean velocity component corresponding to the i direction [m/s]

x_i is coordinate direction i [m]

$$\frac{\partial}{\partial t}(\rho T) + \rho U_j \frac{\partial T}{\partial x_j} = \frac{\partial}{x_j}\left(\gamma \frac{\partial T}{\partial x_j} - \rho u_j T\right) + S_T \qquad (3)]$$

γ is diffusion cofficient

T is fluctuation temprature [℃]

S_T is source term [W/m^3]

$$\frac{\partial}{\partial t}(\rho U_i) + \rho U_j \frac{\partial U_i}{\partial x_j} = -\frac{\partial p}{x_j} + \frac{\partial}{\partial x_j}\left(\mu \frac{\partial U_i}{\partial x_j} - \rho u_i' u_j'\right) + \rho g_i \qquad (4)$$

P is pressure [Pa]

μ is laminar dynamic viscosity [kg/ms]

u_i' is fluctuating velocity component in the i direction [m/s]

g_i is gravitional acceleration in the i direction [m/s^2]

$$\frac{D}{Dt}(\rho\varepsilon) = \frac{\partial}{\partial x_j}\left[\left(\mu + \frac{\mu_t}{\sigma_\varepsilon}\right)\frac{\partial \varepsilon}{\partial x_j}\right] + C_{\varepsilon 1}\frac{\varepsilon}{k} - G_k - \rho C_{\varepsilon 2}\rho\varepsilon \quad (5)$$

k is turbulent kinetic energy [j/kg]

ε is rate of disspiation of turblent kintec energy [j/kg s]

μ_t is turbulent visocity [kg/ms]

G_k is buoyancy term

Constant: $C_{\varepsilon 1} = 1.44, C_{\varepsilon 2} = 1.92, \sigma_\varepsilon = 1.3, \sigma_k = 1.0$

CFD modeling has recently been used in HVAC applications to solve fluid flow and heat transfer issues. Additionally, it offers greater details on air factors (air velocity, air temperature and relative humidity). Standard K-□ model (Eq. 5) with a species transport model were utilized in this numerical computation to address the moisture and air flow properties[53,54]. Turbulence was modeled using K-□ model instead of K-ω model as the interest of this study to model regions far away from walls as K-ω model do better estimate turbulence behavior for flow near wall region. Radiation analysis was conducted through the cooling load calculation by HAP software as it is an imbedded feature inside HAP software. Therefore, the airflow rate used in the boundary conditions has accounted the radiation loads applied to the building through the radiation analysis. Before beginning the meshing process, the physical model was imported into mesh modeler and all geometrical characteristics were examined. Meshing was developed for cells that expand at a rate of 1.2, with a minimum size of 0.1 m and a maximum size of 0.5 m using Mesh modeler of Ansys 19.2. Any defeatures that the geometry design program had provided were removed from the domain. Defeatures was defined to be at least 0.0045 m in size. Moreover, cells were captured

using a minimum size of 0.009 m curvature and a 5.5-degree curvature angle. For 0.08 m cells, the facing mesh tool was applied to the inlet grills, inlet slots, and outlet grills. The pool basin was then treated with 0.07 m cells. The objective of defining different cell sizes at grills and pool basin face is to solve fluid flow equations at those faces and capture them in detail. The unstructured tetrahedral cells had 1869824 elements because of the fine mesh technique, as depicted in (Fig. 9). Calculated values for the minimum, maximum, and average skewness were 0.00036, 0.88, and 0.23. Skewness measurement indicated that mesh was approaching a good meshing procedure. As indicated in Table 2 Mesh metrics, the highest and minimum orthogonal quality values were calculated to be 0.99 and 0.19, respectively. As an excellent quality meshed element in the element quality measure, an average of 0.83 was found. It was crucial to specify the boundary conditions and their various types before beginning any numerical calculations. Supply air inlets were used as mass inflow inlet boundary condition while and return air outlets were assigned as pressure outlet. All other fittings were defined to be walls, with the pool's water surface acting as the mass inflow inlet. The boundary condition of a wall varies depending on the interior fixture, as shown in Table (3) Boundary condition for a swimming pool. The calculation was finally performed using 2000 iterations and a convergence threshold of 0.001. Mesh confirmation test were applied to the model to confirm the independency of the numerical result on mesh size. Figure 10 shows a plot for the average temperature values calculated over the domain volume for each number of elements for five different elements sizes (132676, 832412, 1869824, 2226707 and 3476151 cells). As the number of elements increases, the temperature found to be constant for 24.1 ℃ starting from 832412 to 3476151 cells. 24.2 ℃ was obtained at 132676 cells as the smallest number cells used in mesh validation process. As the results of Figure 10, 1869824 cells and 24.1 ℃ was chosen

for presenting the results of contour planes in the results and discussion for this study.

Table 2 Mesh metrics

Meshing cell size	0.1 m Tetrahedral
Growth rate	1.2
Orthogonal quality (maximum - minimum)	0.99-0.19
Skewness (Maximum - minimum)	0.88-0.00036
Number of Elements	1869824 elements

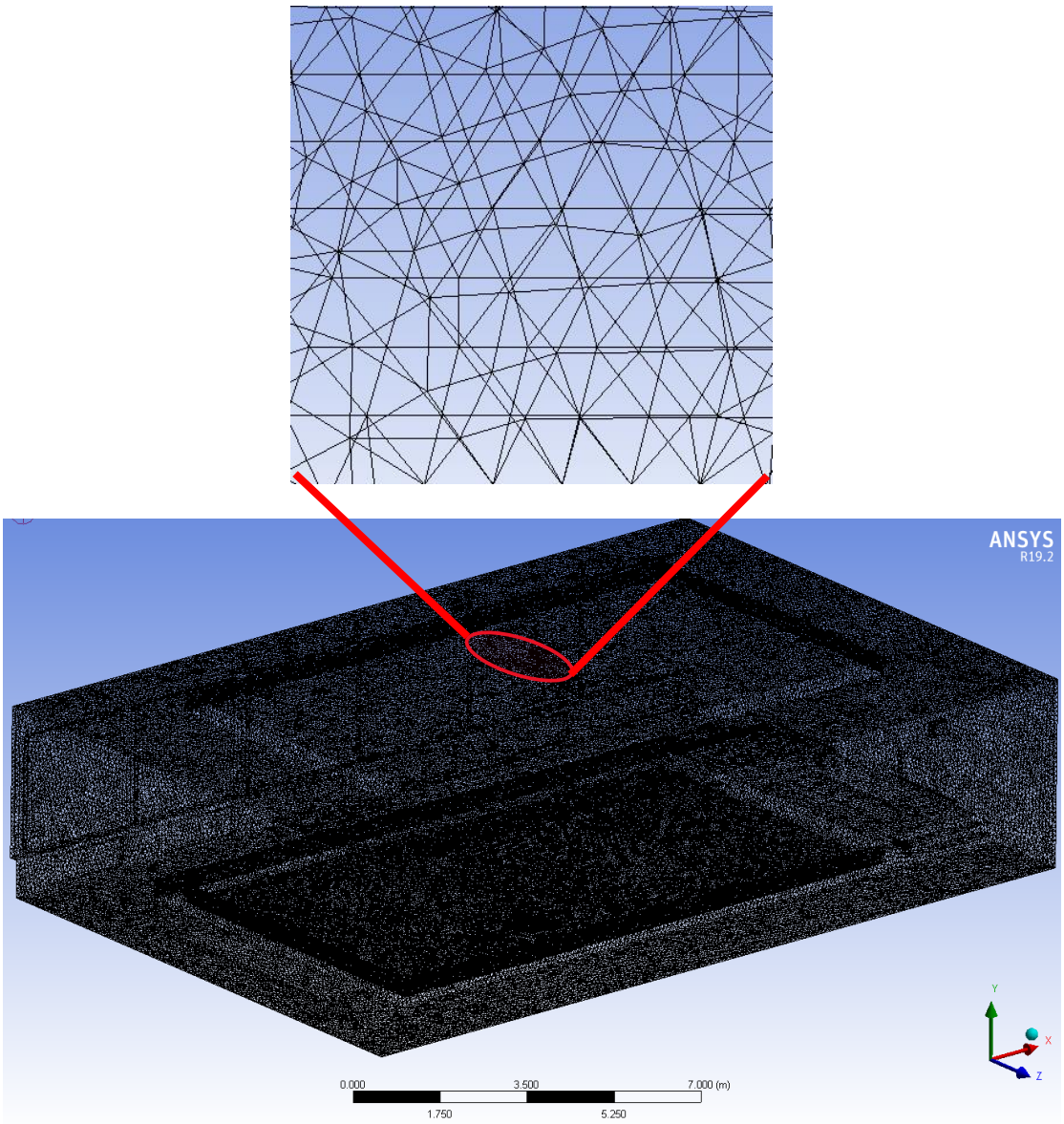

Figure 9. Mesh cells of swimming pool domain.

Table 3 Boundary conditions for swimming pool

Domain element	Boundary condition
Ceiling inlet grills	Mass flow inlet
Inlet slots	Mass flow inlet
Ceiling outlet grills	Pressure outlet
Water surface	Mass flow inlet
Lighting	Wall – Heat flux type

Domain element	Boundary condition
North west wall	Wall – Heat flux type
South west wall	Wall – Heat flux type

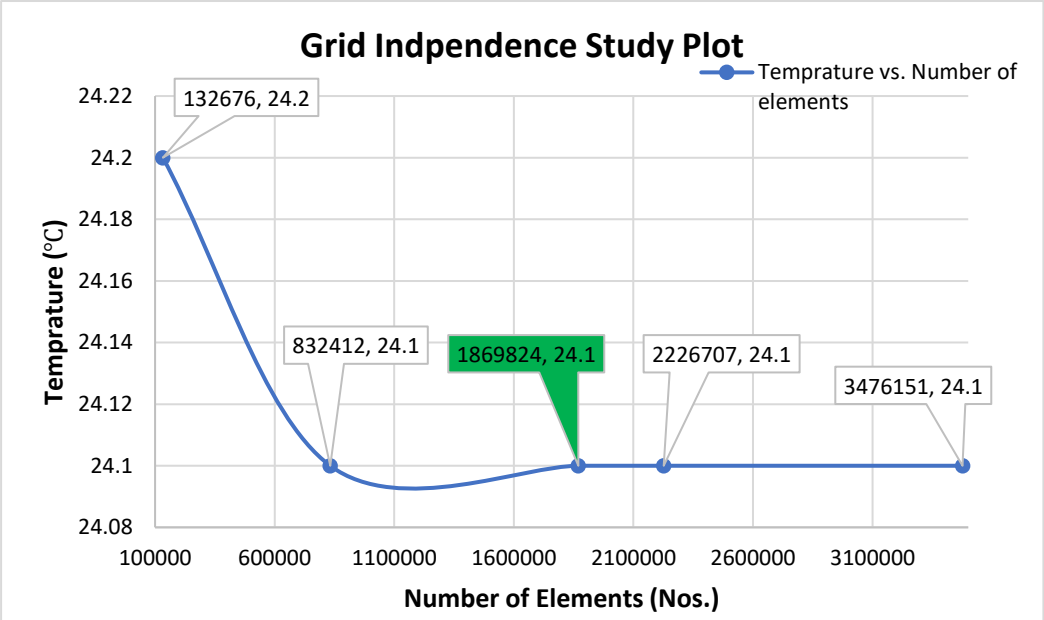

Figure 10. Temperature (℃) vs. Number of elements plot for independence grid study.

3.4 Thermal comfort indices

According to ASHRAE Standard 55, it is necessary to use air variable in determining the comfort of people. For this purpose, two indices are used in studying the thermal comfort: the predicated mean vote (PMV) index and the predicted percentage of dissatisfied (PPD). PMV depend on many variables like metabolic rate (occupant activity level), air temperature, air velocity, partial vapor pressure, mean radiant temperature and clothing temperature. PMV is the heat balance carried on human's

thermoregulatory system where it measures the response of occupant against applied load on the body. It is calculated under steady state conditions with following for comfort (+3) hot, (+2) warm, (+1) slightly warm, (0) neutral, (-1) slightly cool, (-2) cool and (-3) cold. PPD, which measures the satisfaction percentage of the space's occupants, is computed similarly to PMV. Equations 7, 8, 9, 10, and 11 below illustrate PMV and PPD [55–57]. Additionally, Table 3 PMV and PPD parameters provides information on all variables and values utilized in computing PMV and PPD during the summer and winter.

$$PMV = (0.303e^{-0.036M} + 0.028)\{(M - W) - 3.05 \times 10^{-3} \times [5733 - 6.99(M - W) - p_a] - 0.42 \times [(M - W) - 58.15] - 1.7 \times 10^{-5} M(5867 - p_a) - 0.0014M(34 - t_a) - 3.96 \times 10^{-8} f_{cl} \times [(t_{cl} + 273)^4 - (\overline{t_r} + 273)^4] - f_{cl} h_c (t_{cl} - t_a) \quad (7)$$

$$P_s = e^{C_8/T + C_9 + C_{10}T + C_{11}T^2 + C_{12}T^3 + C_{13} lnT} \quad (8)$$

$$C_8 = -5800.2206, C_9 = 1.3914993, C_{10} = -0.048640239, C_{11} = 0.000041764768, C_{12} = -0.000000014452093 \ \& \ C_{13} = 6.5459673$$

$$P_a = RH\% \times P_s \quad (9)$$

$$t_{cl} = 35.7 - 0.028(M - W) - I_{cl}\{3.96 \times 10^{-8} f_{cl} \times [(t_{cl} + 273)^4 - (\overline{t_r} + 273)^4] + f_{cl} h_c (t_{cl} - t_a)\} \quad (10)$$

$$h_c = \begin{cases} 2.38(t_{cl} - t_a)^{0.25} \ for \ 2.38(t_{cl} - t_a)^{0.25} > 12.1\sqrt{v_a} \\ 12.1\sqrt{v_a} \ for \ 2.38(t_{cl} - t_a)^{0.25} < 12.1\sqrt{v_a} \end{cases} \quad (11)$$

$$f_{cl} = \begin{cases} 1.00 + 1.290 I_{cl} \ for \ I_{cl} \le 0.078 m^2.℃/W \\ 1.05 + 0.645 I_{cl} \ for \ I_{cl} > 0.078 m^2.℃/W \end{cases} \quad (12)$$

$$PPD = 100 - 95 \times e^{-(0.03353 \times PMV^4 + 0.2179 \times PMV^2)} \quad (13)$$

M: is the metabolic rate, 46 to 232 W/m^2(0.8 met to 4 met) - 1 met = 58.2 W/m^2

W: is the external work W/m^2, assumed to be 0 for most applications

I_{cl}: is the thermal resistance of clothing, 0 to 0.310 $m^2.℃/W$ (0 to 2 clo) – 1 clo = 0.155 $m^2.℃/W$

t_a: is the air temperature, (10 to 30 ℃)

$\overline{t_r}$: is the mean radiant temperature, (10 to 40 ℃)

v_a: is the air velocity, (0 to 1 m/s)

p_a: is the partial water vapor pressure,

p_s: is the saturation pressure of air, (0 to 2700 pa)

h_c: is the convective heat transfer coefficient in $W/m^2.℃$

t_{cl}: is the surface clothing temperature in ℃

Table 4 PMV and PPD parameters

Parameter	Summer Season	Winter Season
M (W/m^2)	116.4	116.4
I_{cl} ($m^2.℃/W$)	0.3 clo (0.0465$m^2.℃/W$) (Panties, T-shirt, shorts)	0.9 clo (0.1395$m^2.℃/W$) (Shirt, trouser, V-neck sweater)
t_a(℃)	Computed numerically	Computed numerically
$\overline{t_r}$(℃)	t_a(℃) +2.8 ℃ [57]	t_a(℃) +2.8 ℃ [57]

Parameter	Summer Season	Winter Season
v_a(m/s)	Computed numerically	Computed numerically
p_a (pa)	Computed numerically	Computed numerically
h_c $(W/m^2.℃)$	8.725	7.653
t_{cl}(℃)	30.56	28.81

PMV index scale:
Hot (+3) – Warm (+2) – Sligthly warm (+1) – Neutral (0) – Slightly cool (-1) – Cool (-2) - Cold (-3)
Recommended range for thermal comfort: PMV (-0.5 < PMV<0.5) and PPD (PPD<10%)

CHAPTER 4: MANAUAL CALCULATIONS,

RESULTS AND DISCUSSION

This chapter is divided into three parts. In the first section, manual cooling load calculation will be prepared and compared with the computed one of HAP software, Details of material and information used to conduct the calculation were discussed in section 4.1 thermal load calculation. Validation results of Ciuman et al. [41] model is presented and compared with Ciuman et al. [41] measurement (experimental) and numerical work. The final section of this thesis is showing the result of numerical study for the validated model being implemented in Qatar as a hot and arid environment country. Then, the results were discussed to verify its compliance with AHSRAE standards recommendations for indoor conditions in indoor swimming pools. In addition to studying the thermal comfort indices (PMV and PPD) for the space using Franger's model.

4.1 Thermal load calculation

In this section manual Cooling load procedures will be explained briefly using the information which has been discussed in section 3.2 Thermal loads. Total cooling load are divided into sensible and latent loads. Sensible loads are loads dissipated from people, ventilation, lighting, wall, glazing and roof while latent loads are obtained from people, ventilation and evaporation of pool water surface. On the other hand, total heating load was computed for winter season was found to be minimal, so it was not considered in the analysis of this study. However, air flow for heating load computed from HAP were used as filtration to space in the numerical analysis of winter season. Moreover, each load source will be computed separately then all load sources will be

added to compute the total cooling load. Equation used for calculating thermal loads for each load source is defined in table 5 Thermal equations and load source summary.

Table 5 Thermal equations and load source summary.

Load Source	Equation	Refernece
Roof	$Q\ (btu/hr) = U \times A \times CLTD$	Table 11.1 ASHRAE Pocket guide 9th [58]
Wall	$Q\ (btu/hr) = U \times A \times CLTD$	
Glazing (Conduction load)	$Q\ (btu/hr) = U \times A \times CLTD$	
Glazing (Radiation load)	$Q\ (btu/hr) = A \times SC \times SCL$	
People (Sensible load)	$Q\ (btu/hr) = N \times SHG \times CLF$	
People (Latent load)	$Q\ (btu/hr) = N \times LHG$	
Lighting (Sensible load)	$Q\ (btu/hr) = q_l \times blt \times CLF$	
Ventilation (Sensible load)	$Q\ (btu/hr) = 1.10 \times CFM \times \Delta t$	
Ventilation (Latent load)	$Q\ (btu/hr) = 4840 \times CFM \times \Delta W$	
Thermal Resistivity(R-value)	R-value $(ft^2°F/btu/hr) = \frac{1}{U-value}$	

U: U-value (Thermal conductivity, btu/hr/ft^2°F)
A: Area, ft^2
CLTD: Cooling Load Temperature difference, °F
SC: Shading Coefficient, unitless
SCL: Solar Cooling Load Factor, °F
N: number of people, nos.
SHG: Sensible Heat Gain Factor, btu/hr/person
CLF: Cooling Load Factor, unitless
LHG: Latent Heat Gain Factor, btu/hr/person
blt: Ballast multiplier, unitless
q_l: Lighting Power Density, W/ft^2
CFM: Ventilation air flow, CFM
Δt : Outdoor and indoor design temperature difference
ΔW : Outdoor and indoor design humidity ratio difference

Thermal loads were computed on hourly basis through each source and then added all together to determine the peak hourly load. Wall and Roof were considered to have conduction heat transfer process while glazing had a conduction and radiation heat transfer process. Wall, Roof and Glazing thermal conduction loads are determined using cooling load temperature difference (CLTD) which is a temperature difference

across an element for each solar time (hour) of space occupation. CLTD tables are classified by the latitude of country, the latitude of Qatar is 25.6° N which can be approximated to 24° N as the available CLTD tables are in 24° N, 36° N and 48° N. CLTD values were corrected as CLTD tables available from ASHRAE standards were constructed under conditions of indoor temperature 78°F and outdoor mean temperature 85°F. Correction equation for CLTD were defined Table 11.13, P.225 AHRAE Pocket guide 9th as shown in (Eq.14) [58]. Radiation thermal load for glazing was determined using solar cooling load factor (SCL) at 24°N. SCL values was also changing with solar time as CLTD tables for conduction loads. In addition to SCL, shading coefficient (SC) was obtained and used in radiation load calculation according type of glass being used, simply SC describes the amount of solar heat gain that could pass by glazing into the air-conditioned room. Thermal loads of People and lighting were computed using cooling load factors (CLF) in Table 37-38, P. 637-638 ASHRAE Fundamental Handbook 1997[59]. Cooling load factor determines the percentile of people occupying and lights which are operating during the operation hours of the air-conditioned room. Heat dissipation factors (w/ft^2) defined in Table 11.13-11.17, P.228-230 ASHRAE Pocket guide 9th were then used with CLF to calculate People and lighting loads. Ventilation loads were calculated using outdoor air flow with indoor and outdoor condition of humidity ratio and temperature to obtain the required loads for fresh air in breathing zone. Outdoor air flow requirement (cfm/ft^2) was selected for a category of sports arena (sub-category: play area) from Table 6-1, ASHRAE standard 62.1. In order to calculate each load source, other space input information was required to be defined as shown in Table 6.

$$CLTD_{Corrected}(°\text{F}) = CLTD + (78 - t_r) + (t_m - 85) \quad (14)$$

t_r(°F): $indoor\ temprature$

$$t_m(°\text{F}) = maxiumum\ outdoor\ temprature - \frac{daily\ range}{2}$$

Table 6. Space input information.

Country	Qatar	reference
Location (Latitude)	25.6°N	Chapter climate design, ASHRAE Fundamental Handbook 1997 [59]
Summer Outdoor temperature DB/WB (°F)	109.4/91.94	(Sleiti et al., 2022) [44]
Indoor Conditions DB (°F) / RH%	74.3 °F /50%	Indoor swimming pools ,ASHRAE applications handbook 2019 (Eq.1) [46]
Daily range temperature DB (°F)	51.44	Chapter climate design, ASHRAE Fundamental Handbook 1997 [59]
Operation hours (hrs)	8:00 a.m to 18:00 p.m	Swimming pool duty hours in Qatar
Occupant Load	14 persons	Table 6-1, Ashrae standard 62.1 (sub-category: play area) [45]

4.1.1 Wall and Roof Loads

Heat dissipation from structural elements such as Roof and walls requires defining the heat transfer coefficient (U-value) and cooling load temperature difference (CLTD). U-value for walls and roofs were defined to be 0.100 and 0.077 btu/hr/ft^2°F respectively as per Kharama standard (energy and water conservation code, section 05: thermal insulation of building p.11) as discussed in Table 1, section 3.2 thermal loads. The specified U-value were used in calculating Thermal resistivity (R-value = 1 / U-value) which will be used in describing the Composite of materials used for roof and walls construction. The Total R-value (1 / Total U-value) for walls and roof were computed as 10 (1 / 0.100) and 12.98 (1 / 0.077) ft^2°F/btu/hr as shown in Table 7 Total R-value for wall and roof. The R-value of component in wall and roof assembly were extracted from R-value data of Table 11 P.605 ASHRAE Fundamental Handbook 1997 [59].

Then, R-value of each material were added to achieve the total R-values value calculated earlier for wall and roof. The assembly of wall and roof materials were designed to show their components as shown in Figure 10a and 10b. To obtain CLTD and Thermal loads of roof, Table 11.10, p.223 AHRAE Pocket guide 9th [58] was used with the calculated roof R-value 12.98 ft^2°F/ btu/hr to define a Roof number. Roof number which will be used later in obtaining CLTD for each solar hour (space operation hours). Roof number 4 has been extracted from Table 11.10 and used in Table 11.7, p.222 AHRAE Pocket guide 9th[58]to obtain CLTD value. Corrected CLTD were calculated, and thermal loads were obtained accordingly using Roof thermal load equation in Table 5 for a roof area 2216.3 ft^2 . Figure 11 shows the selected solar time for Roof number 4 using Table 11.7, p.222 AHRAE Pocket guide 9th [58]. Roof thermal loads are presented in Table 8 Roof Thermal Loads. The same procedure for obtaining roof number and CLTD were applied to wall where wall number 2 was obtained from Table 33A P.632 ASHRAE Fundamental Handbook 1997 [59] via R-value 10 ft^2°F/ btu/hr. Then, Table 11.11, p.224 AHRAE Pocket guide 9th [58]was used with exposed walls being directed to North west (NW) and south west (SW). NW and SW were used obtain CLTD for each solar hour from Table 11.1. Wall thermal loads were calculated using corrected CLTD and exposed wall area of 429.66 ft^2 in SW and 554.3 ft^2 in NW directions as shown in Table 9 Wall Thermal loads. Other walls were designed to be internal partitions to air-conditioned zone.

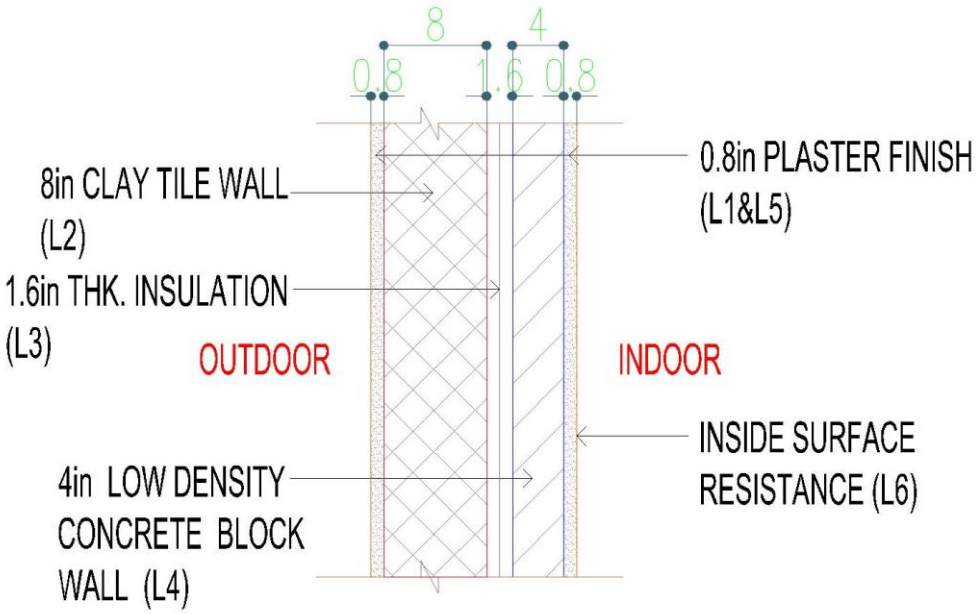

(a)

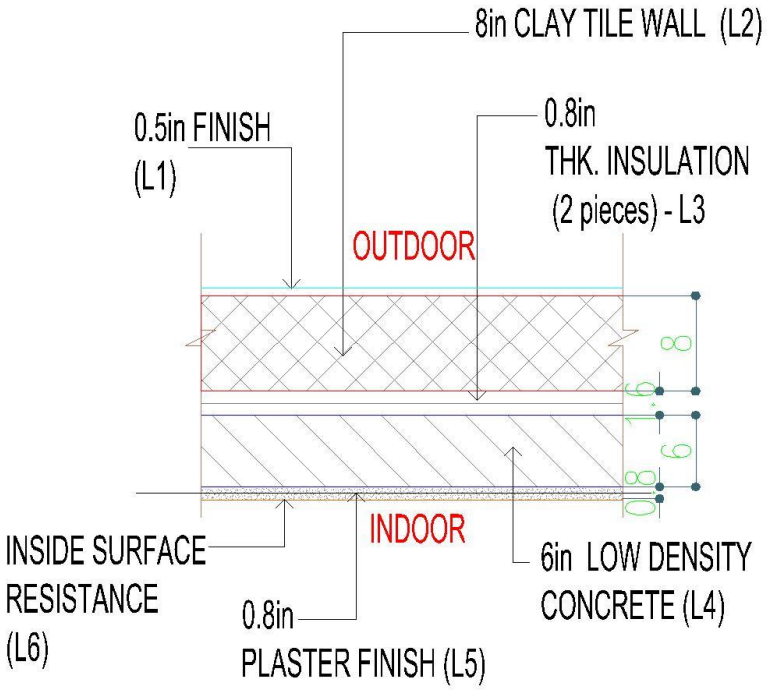

(b)

Figure 11. Assembly of materials for (a) Wall and (b) Roof .

Table 7 Total R-value for wall and roof

Wall

Layer number	Description	Thickness (inch)	R-value (ft^2°F/btu/hr)
L1	0.8-inch Plaster finish	0.8	0.147
L2	8-inch Clay Tile	8	2
L3	1.6-inch insultation	1.6	5.5
L4	4-inch low density concrete block	4	1.510
L5	0.8-inch Plaster finish	0.8	0.147
L6	Inside surface resistance	0	0.687
	Total	15.2	10

Roof

Layer number	Description	Thickness (inch)	R-value (ft^2°F/btu/hr)
L1	Finish	0.5	0.15
L2	8-inch Clay Tile	8	2
L3	0.8-inch insultation x 2 pieces	1.6	5.5
L4	6-inch low density concrete	6	4.5
L5	0.8-inch Plaster finish	0.8	0.147
L6	Inside surface resistance	0	0.687
	Total	16.9	12.98

Table 11.7 CLTDs for Flat Roofs—24°N Latitude, July

Roof No	Solar time, h											
	2	4	6	8	10	12	14	16	18	20	22	24
1	–2	–5	–6	9	44	76	92	86	58	23	8	2
2	0	–4	–6	1	30	64	86	89	70	36	14	5
3	8	2	–2	3	22	47	68	77	68	47	29	16
4	11	3	–2	–4	5	27	55	75	80	67	43	23
5	16	8	3	1	10	30	52	68	70	59	41	27
8	24	17	11	9	14	27	43	54	58	52	42	32
9	25	16	9	4	5	17	36	54	65	63	51	37
10	31	22	15	9	8	16	30	45	56	59	52	41
13	31	25	20	16	16	23	33	43	49	49	43	37
14	32	27	23	19	19	24	32	40	45	45	42	37

Figure 12 Table 11.7, p.222 AHRAE Pocket guide 9th [58]

Table 8 Roof Thermal Loads

Time	CLTD	CLTD corrected (°F)	Q(Btu/hr)
8	-4	-1.62	-276.46
10	5	7.38	1259.43
12	27	29.38	5013.85
14	55	57.38	9792.19
16	75	77.38	13205.29
18	80	82.38	14058.57

Table 9 Wall Thermal loads

Time	SW CLTD	CLTD corrected (°F)	Q(Btu/hr)
8	-1	1.38	59.29
10	5	7.38	317.09
12	13	15.38	660.82
14	24	26.38	1133.44
16	42	44.38	1906.83
18	54	56.38	2422.42
Time	NW CLTD	CLTD corrected	Q(Btu/hr)
8	-1	1.38	76.49
10	5	7.38	409.07
12	13	15.38	852.51
14	22	24.38	1351.38
16	40	42.38	2349.12
18	60	62.38	3457.72

4.1.2 Glazing Loads

Conduction heat transfer of windows were calculated using corrected CLTD from CLTD values of Table 34 p. 635 ASHRAE Fundamental Handbook 1997 [59]. six windows with area of 403.44 ft^2 per window were using in calculating glazing thermal loads. U-value of 0.370 btu/hr/ft^2°F was defined in section 3.2 thermal loads as per QCS standard (Section 05: Insulation of building, Part 02: Building insulation, p. 4). Then, Table 5, p.659 ASHRAE handbook fundamental 1997 [59] was used to select the glazing type (double glazing, ½ inch argon space) via the obtained R-value (1 / 0.370 = 2.7 ft^2°F/ btu/hr). Moreover, all obtained information of window area, U-value and corrected CLTD were used to calculate conduction thermal load through glazing as shown Table 10 Glazing Conduction Thermal loads. On the other hand, radiation heat loads were calculated using solar cooling load (SCL) instead of CLTD values which

was taken from Table 11.14, p.226 ASHRAE Pocket guide 9th [58].A screen shot of the selected SCL were taken from Table 11.14, p.226 ASHRAE Pocket guide 9th [58]as presented in Figure 12. Then, radiation thermal loads were determined using hourly solar cooling load factor for windows facing southwest and shading coefficient of 0.4 (section 3.2 thermal loads) as shown in Table 11 Glazing Radiation Thermal loads

Table 10 Glazing Conduction Thermal loads

Time	Conduction CLTD	CLTD corrected (°F)	Q(Btu/hr)
8	0	2.38	355.27
10	4	5.98	892.65
12	9	11.38	1698.72
14	13	14.98	2236.11
16	14	16.78	2504.80
18	13	14.98	2236.11

Table 11.14 Solar Cooling Load for Sunlit Glass (SCL)

Tables do not consider zone type and are conservative. Use for preliminary computations only.

Glass Facing	Solar time, h																	
	5	6	7	8	9	10	11	12	13	14	15	16	17	18	19	20	21	22
24°N Latitude, July																		
N	0	19	35	36	36	38	40	42	42	40	38	39	43	32	11	6	3	1
NE	0	54	124	150	144	115	78	58	49	44	38	32	25	14	6	3	1	1
E	0	57	139	177	180	154	107	68	54	46	40	33	25	14	6	3	1	1
SE	0	26	74	104	114	106	83	59	50	44	38	32	25	14	6	3	1	1
S	0	5	15	23	30	35	40	43	43	40	37	32	24	14	6	3	1	1
SW	0	5	15	23	30	35	39	42	61	88	110	118	105	62	24	12	6	3
W	0	5	15	23	30	35	39	41	67	116	160	186	184	118	44	21	11	5
NW	0	5	15	23	30	35	39	41	51	83	122	151	158	106	39	19	9	5
Hor	0	10	55	113	170	218	253	271	273	258	225	176	115	54	24	12	6	3

Figure 13. Table 11.14, p.226 AHRAE Pocket guide 9th[58].

Table 11 Glazing Radiation Thermal loads

Time	SCL	SC	Q(Btu/hr)
8	23	0.4	3711.65
10	35	0.4	5648.16
12	42	0.4	6777.79
14	88	0.4	14201.09
16	118	0.4	19042.37
18	62	0.4	10005.31

4.1.3 People, Lighting and Ventilation Loads

Thermal loads of people and outdoor fresh air (Ventilation load) have shared the same properties in adding sensible and latent heat loads to the space. While lighting thermal load has added only sensible loads to the space. In order to obtain sensible loads for lighting, cooling load factor (CLF) was required to be obtained on hourly basis from Table 38, p. 638 ASHRAE handbook fundamental 1997 [59]. CLF values selection depends on the type of zone (A,B, Cand D) which is categorized by the interior furnishing of the space such as floor covering, number of exposed walls, partition material type. The type of zone was selected as Type C from ASHRAE handbook fundamental 1997, Table 35B p.635 [59]. Zone C was selected for vinyl as floor covering and concrete block as partition material type. Then, it was required to define the type of lighting to obtain ballast multiplier as the final step in Lighting thermal load calculation as shown in table 12 lighting thermal loads. Ballast multiplier was obtained 1.0 for a florescent type light with light power density of 0.44 W/ft^2 (section 3.2 thermal loads, Table 11.17 Lighting Thermal loads p. 230 ASHRAE Pocket guide 9th [58]) for space area 2216.3 ft^2. People thermal loads were divided into sensible and latent loads which was calculated according to the activity level of humans in the space. Moreover, sensible heat gain factor (SHG) and latent heat gain factor (LHG) were obtained as 710 and 1090 btu/hr/person respectively for Athletics activity from Table

11.16, p.228 ASHRAE Pocket guide 9th [58]. CLF values were only applied to sensible heat gain while latent heat gain was directly applied to occupant load (14 persons) without applying CLF values. CLF were obtained for people sensible loads from Table 37, p. 637 ASHRAE handbook fundamental 1997[59]. People sensible and latent thermal loads were calculated as displayed in Table 13 People Thermal loads. On the other hand, ventilation load (Fresh air load) was introduced in total loads by supplying fresh air into the space. Fresh air load was calculated using outdoor air flow rate based on the indoor quality of ASHRAE standard 62.1, Table 6-1 p. 22 [45]. Outdoor floor rate was calculated as 664.89 CFM using sport arena category as defined in ASHRAE standard 62.1 for value of 0.3 CFM/ft^2 and as discussed in section 3.2 thermal loads. Furthermore, sensible load of ventilation was calculated using the temperature difference of outdoor and indoor conditions which is defined in Table 6 space input information. But latent load was computed via obtaining the difference in humidity ratio of indoor and outdoor conditions. Both conditions of humidity ratio were extracted from psychrometric chart using two inputs for each condition as described Table 6 space input information. It was found to be 0.028811 and 0.009019 Ib/Ib dry air for outdoor condition and indoor condition respectively. Ventilation thermal load was calculated via combining sensible and latent load as shown in Table 14 Ventilation thermal loads.

Table 12 Lighting Thermal loads

Time	Lights Power (Watts)	ballast multiplier	CLF	$Q_{(Btu/hr)}$
8	975.17	1	0.81	2685.62
10	975.17	1	0.87	2884.56
12	975.17	1	0.90	2984.03
14	975.17	1	0.92	3050.34
16	975.17	1	0.93	3083.49
18	975.17	1	0.16	530.49

Table 13 People Thermal loads

Time	SHG (btu/hr)	LHG (btu/hr)	CLF	Qs(Btu/hr)	Ql(Btu/hr)	Qt(Btu/hr)
8	710	1090	0.90	8946	15260	24206
10	710	1090	0.93	9244.20	15260	24504.20
12	710	1090	0.95	9443	15260	24703
14	710	1090	0.97	9641.80	15260	24901.80
16	710	1090	0.98	9741.20	15260	25001.20
18	710	1090	0.99	9840.60	15260	25100.60

Qs: sensible thermal load , Ql: Latent thermal load and Qt: Total Thermal load

Table 14 Ventialtion Thermal loads

Time	Qs(Btu/hr)	Ql(Btu/hr)	Qt(Btu/hr)
8	25671.40	63691.99	89363.40
10	25671.40	63691.99	89363.40
12	25671.40	63691.99	89363.40
14	25671.40	63691.99	89363.40
16	25671.40	63691.99	89363.40
18	25671.40	63691.99	89363.40

Qs: sensible thermal load , Ql: Latent thermal load and Qt: Total Thermal load

4.1.4 Total Thermal Load

In this section, total thermal was calculated through all thermal loads obtained by people, ventilation, lighting, glazing, wall, and roof as shown in Table 15 Total thermal load. Then air flow required to maintain thermal comfort and indoor conditions were calculated using total sensible thermal load and the temperature difference between entering and supply air temperature of AC system cooling coil (83.9 and 54.2 °F,respectively). The Peak thermal load was calculated 202661 btu/hr (17.73 Ton of Refrigerant) at 16:00 p.m. and Air flow was calculated as 2657.9 CFM at 85256 btu/hr peak sensible load. On the other hand, peak thermal load and air flow were calculated from HAP as 17.6 TR (Ton of Refrigerant) and 2785 CFM. The absolute error was calculated between HAP and manual calculation results to verify

the manual cooling load calculation. 0.75 % absolute error were determined for total thermal load and 4.5% for air flow. Apart from that, Psychometric process for air conditioning system was plotted on psychrometric chart using all indoor, outdoor conditions and manual cooling load calculation results as presented in Fig 14.

Table 15 Total thermal load

Time	Roof	Wall	Glazing	Lighting	People	Ventilation	Total
8	-276	136	4067	2686	2686	89363	166385
10	1259	726	6541	2885	2885	89363	171483
12	5014	1513	8477	2984	2984	89363	178258
14	9792	2485	16437	3050	3050	89363	192234
16	13205	4256	21547	3083	3083	89363	202661
18	14059	5880	12241	530	530	89363	193379

Notes: -

- All thermal loads are in Btu/hr
- Thermal loads for Exposed walls in northwest and south west were added together for each solar hour
- Glazing thermal conduction and radiation loads were added together for each solar hour
- Pool latent load were calculated as per section 3.2 thermal load to be 46204 btu/hr for each solar hour, so it is added for each hourly total load

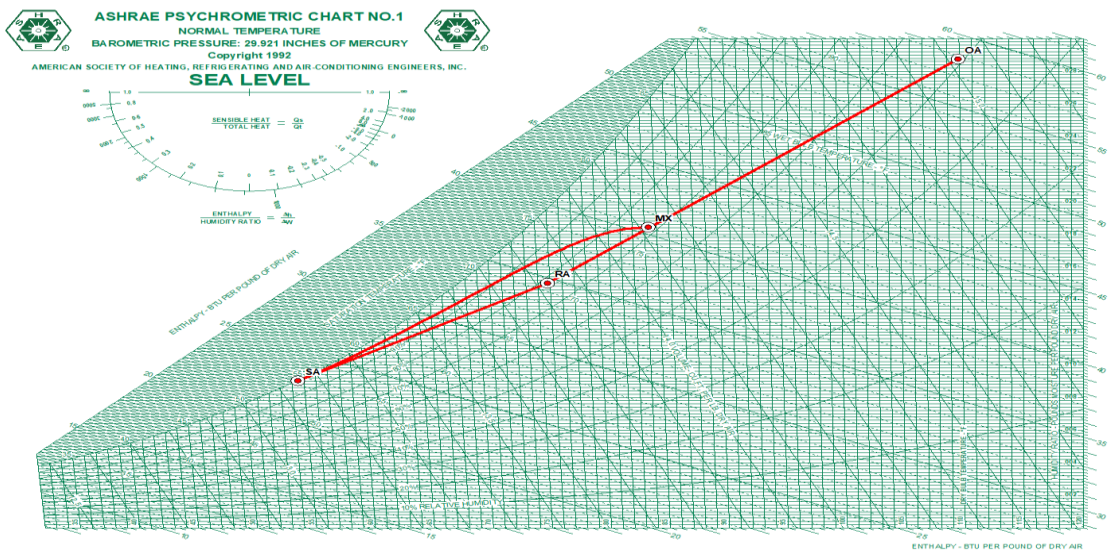

Figure 14. Phschromteric process for swimming pool (OA: outdoor air, MX: mixed air, SA: supply air and RA: return air).

4.2 Validation results

The swimming pool model used in this study was modelled using Ansys Fluent 19.2 and the boundary conditions were taken as described in Ciuman et al. [41] study. Validation was conducted and results are discussed so the same model can be used for the thermal comfort and air variable analysis in Qatar environmental conditions. The computed results for validated model and Ciuman et al. work is presented in the contour plots (Fig. 15-17) and air variables (air temperature, air velocity and relative humidity) graphs in (Fig. 18-20). Contours plot (Fig. 15-17) were discussed for plane at 0.6 m while air variables graph (Fig. 18-20). were plotted for all heights (0.1, 0.6, 1.1 and 1.7 m) as presented by Ciuman et al. [41] in his study. The results of Ciuman et al. [41] were prepared for April 2015 (case 1), June 2015 (case 2), and February 2016 (case 3).

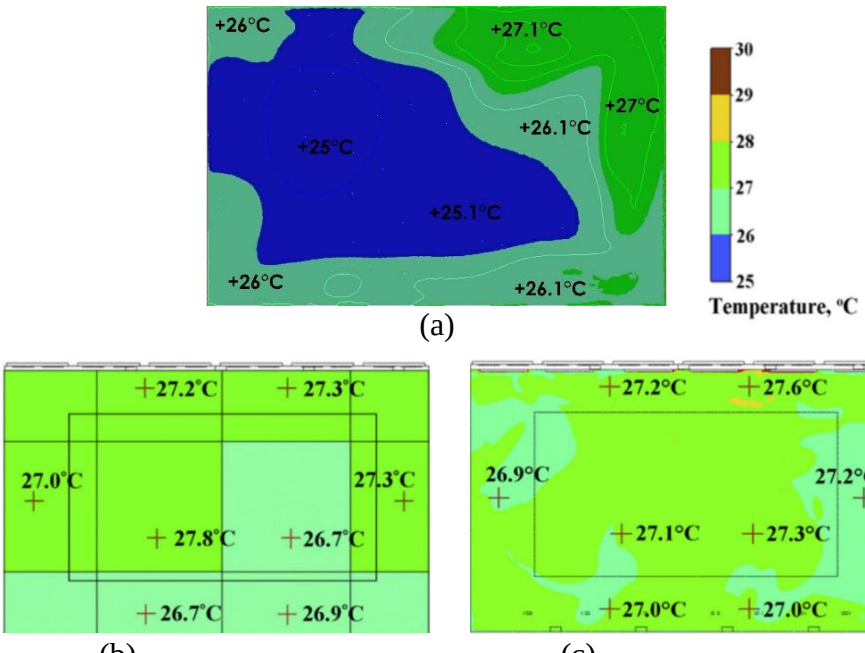

Figure 15. Comparison of Temperature contours of (a) validation results with (b) Ciuman et al. measurement result [41] and (c) numerical simulation of Ciuman et al.[41].

It is clearly shown that measurements (Fig. 15b) and CFD results (Fig. 15c) are in line with each other, where the average temperature was obtained 27℃ in each plot. In contrast, the Validated CFD results showed an average temperature of 26℃ (Fig. 15a). The highest temperature was determined for all figures near the glazing area because it is exposed to high radiation load compared to other areas. (Fig. 15a) has differed from other plots with a decrement of 2℃ in the part covering basin area. The absolute error was obtained as 5% for this area. Apart from that, it is shown that there is not any temperature difference was expressed between pool basin and walking space. Even though, measurement of temperature showed 29 for the region above water surface. In (Fig. 15a), all plots are showing that the temperature decreases gradually from room walls towards pool basin. In overall, the average temperature for (Fig. 15a) was determined to be 26℃ which is less than 5% deviation from measurement and Ciuman et al. [41] results.

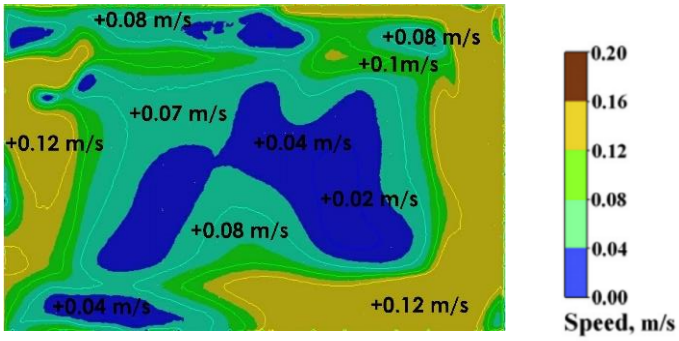

(a)

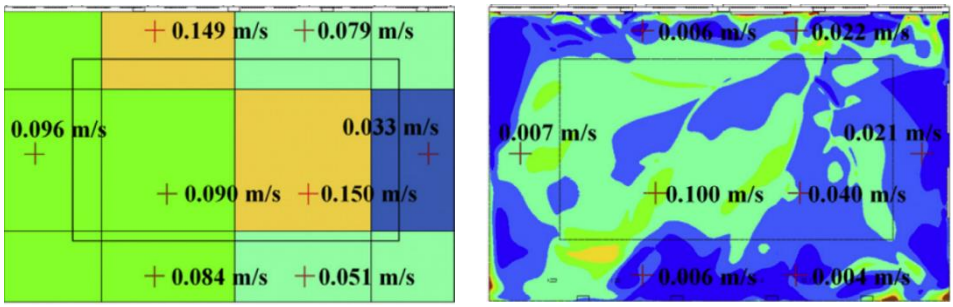

(b) (c)

Figure 16. Comparison of Velocity contours of (a) validation results with (b) Ciuman et al. measurement result [41] and (c) numerical simulation of Ciuman et al.[41].

As presented in (Fig. 16a), the average velocity for validated simulation was determined 0.08 m/s as same as the average measured velocity obtained by Ciuman et al. [41] in (Fig. 16b). On the other hand, the average velocity of numerical study done by Ciuman et al. [41] was obtained as 0.02 m/s (Fig. 16c) which has been found to be away from the average air velocity shown in (Fig. 16a) and (Fig. 16b). In other words, numerical study of Ciuman et al. [41] produced a velocity that is one-fourth the average velocity obtained in (Fig. 16a) and (Fig. 16b). All figures had agreed to have a range of velocity 0.08 – 0.1 m/s in the area above pool basin. (Fig. 16a) showed a uniform distribution of velocities as it increases gradually form the water surface to room walls. Lower velocities were investigated above pool basin area because water evaporation was mixed with forced air limiting its speed. Contours plot of (Fig. 16a) and (Fig. 16b) showed a similarity in air velocity distribution for walking path region. The average air

velocities were determined 0.12 and 0.096 m/s for (Fig. 16a) and (Fig. 16b) respectively in the left-hand side of contour plane. The highest air velocity was found in the measurement case as 0.15 m/s and in numerical simulation as 0.1 m/s of Ciuman et al. [41] study. In contrast, it was obtained as 0.12 m/s in the validation contours. As an overall observation, the validation results (Fig. 16a) for air velocity were considered to best fit the measurement results (Fig. 16b) compared to the numerical results (Fig. 16c) of Ciuman et al. [41]

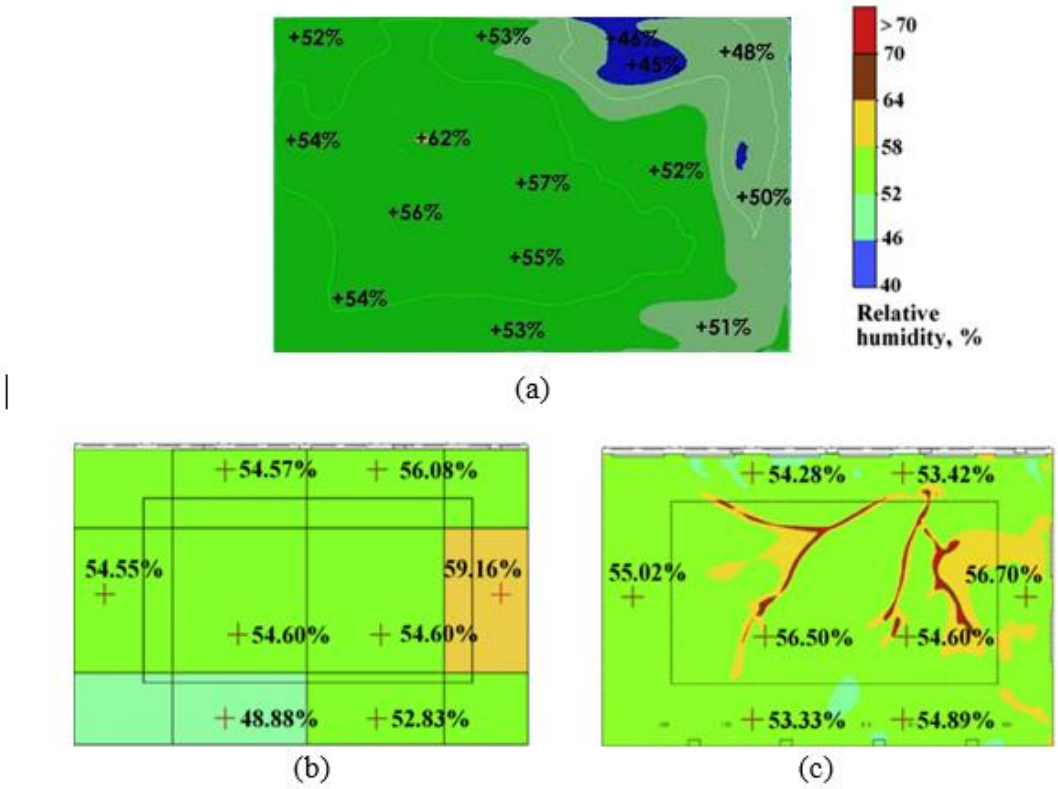

Figure 17. Comparison of Relative humidity (RH) contours of (a) validation results with (b) Ciuman et al. measurement result [41] and (c) numerical simulation of Ciuman et al.[41].

High evaporation rates of water can be observed clearly in (Fig. 17a) compared to other figures. 62% RH was obtained as the highest RH at the center of contour plane. On the other hand, (Fig. 17c) has showed high evaporation rates as more points were indicated

to be higher than 70% RH above pool basin. The highest RH percentages in (Fig. 17b) was found to be 59.16% near the North-west exposed wall. This means that both (Fig. 17a) and (Fig. 17b) are in range of the highest Relative humidity compared to (Fig. 17c). Thus, validation (Fig. 17a) and measurement (Fig. 17b) results were approximately equal in their contours compared to Ciuman et al. [41] numerical results (Fig. 17c). The average relative humidity for (Fig. 17a) was computed as 51.1% which around 6-7% away from the numerical (Fig. 17c) and measurement results (Fig. 17b). These error percentage was calculated by the average relative humidity 55% for numerical simulation (Fig. 17c) and 54.5% for measurement (Fig. 17b). Both (Fig. 17a) and (Fig. 17b) were showing similar values for the lowest relative humidity which was calculated 48.88%. On the other hand, (Fig. 17a) and (Fig. 17c) showed similar relative humidity 53% in the North-east near boundary wall area.

Further to the comparisons made on contour plots, it was vital to discuss the validation results in more details to ensure that the validated model is useful and beneficial for this study. Therefore, a discussion was prepared on the results for air flow parameters (air velocity, air temperature and relative humidity) between Ciuman et al. [41] measurements, Ciuman et al. [41] numerical simulation and current validation results at four heights 0.1, 0.6, 1.1 and 1.7 m. A plane was taken in the current validation study by Ansys fluent 19.2 at each height. To calculate the mean values for all air flow parameters (air temperature, air velocity and relative humidity) and compare it with results of Ciuman et al. [41] measurements, Ciuman et al. [41] numerical simulation. This operation was done for the three measurement cases being tested by Ciuman et al. [41] in his study. A comparison made among all air flow parameters showed that air speed results were having the lowest errors compared to relative humidity and air temperature.

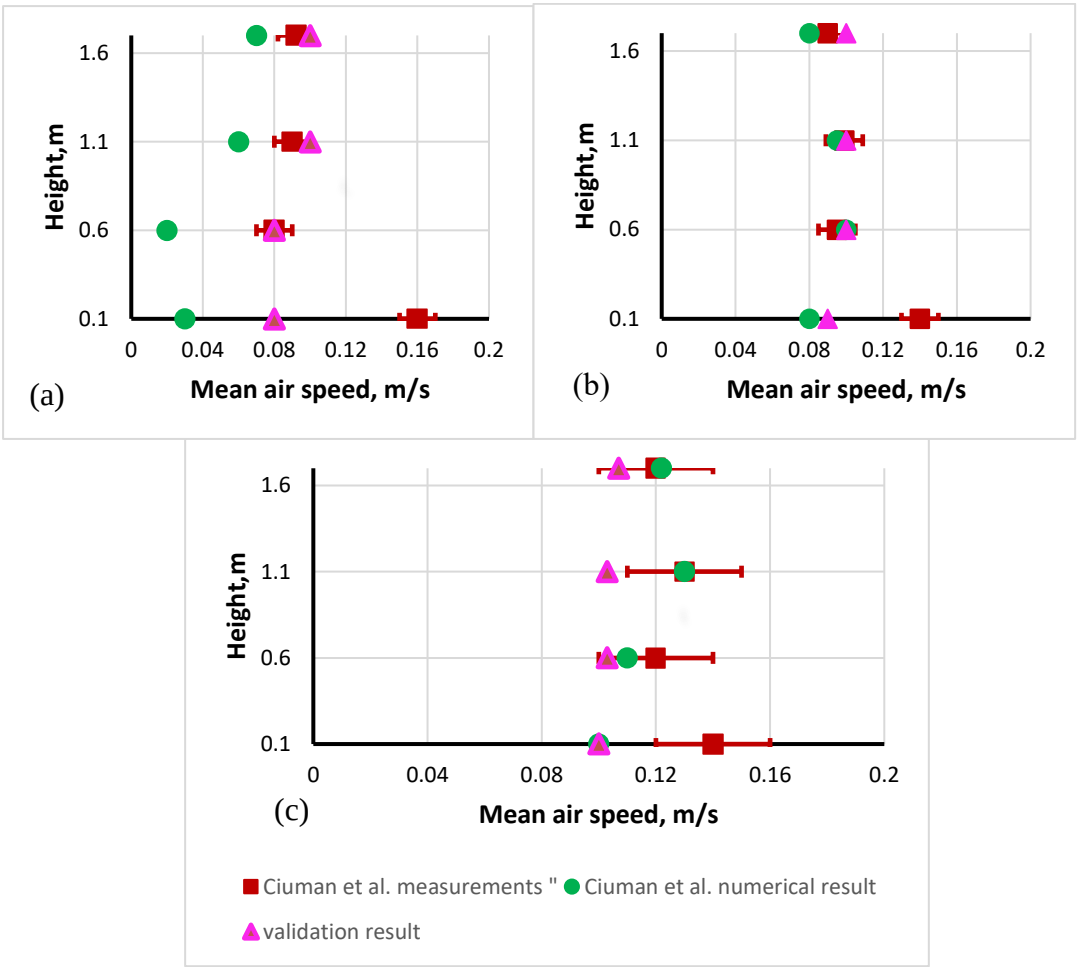

Figure 18. The Comparison of results for Ciuman et al. measurements [41], Ciuman et al. numerical result [41] and validation result for mean air speed at four different heights for a) case 1, b) case 2, c) case 3.

It is noticeable from (Fig 18) that all cases have shown good results where error percentage was minimized especially for case 1 and 2. In case 1 (Fig 18a, case 1), validation result had 0.08 m/s air velocity as same as Ciuman et al. [41] measurement at height 0.6 m. While height 0.1 m showed that validation result is almost half of the Ciuman et al. [41] measurement. Moreover, 8.7-11 % error was obtained at height 1.1 and 1.7 m between Ciuman et al. [41] measurement and validation results which was found to occur at velocity range 0.09-0.1 m/s. In (Fig. 18b, case 2), results of validation

work and Ciuman et al. [41] numerical work showed to be identical which indicates high accuracy of validation result in achieving the results of Ciuman et al. [41] numerical result. Except a deviation was obtained by Ciuman et al. [41] measurement against the other approaches at height 0.1 m. The average air velocity was calculated 0.14 m/s while it was found to be 0.1 m/s for validation and Ciuman et al. [41] numerical results at the same height 0.1 m. Furthermore, there was no error between obtained at 0.6 m (mean air velocity = 0.1 m/s) between validation and Ciuman et al. [41] numerical results. However, 5.26% absolute error was found with Ciuman et al. [41] measurement. For height = 1.1 m, 1% absolute error was calculated between validation and Ciuman et al. [41] measurement. In contrast 5.26% error was computed between validation result and Ciuman et al. [41] numerical results at the height 1.1 m. The third case (Fig 18c, case 3) showed small difference between all approaches and validation results for all heights. The difference was found to be 0.04, 0.023, 0.03 and 0.027 m/s for 0.1, 0.6, 1.1 and 1.7 m height. Even though, Ciuman et al. [41] measurements showed to follow similar deviation obtained in (Fig. 18b, case 2) at height 0.1 m as air velocity obtained 0.14 m/s and 0.1 m/s in validation result and Ciuman et al. [41] numerical results.

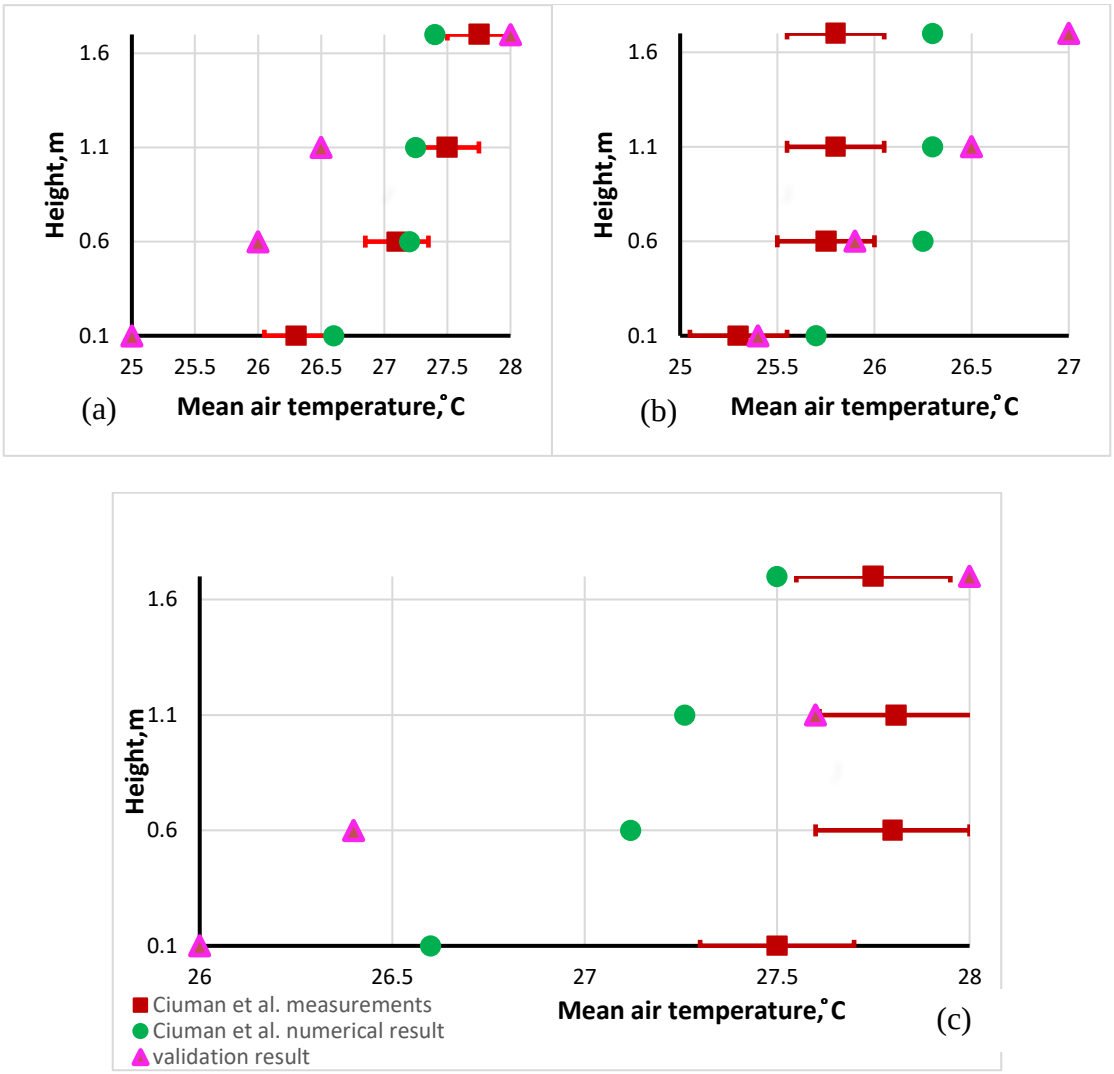

Figure 19. The comparison of results of Ciuman et al. measurements [41], Ciuman et al. numerical result [41] and validation result for mean air temperature at four different heights for a) case 1, b) case 2, c) case 3.

The use of temperature variable in comparing between cases showed high accuracy for all results at tow heights only 1.1 and 1.7 m. The highest error was obtained 6% between validation and Ciuman et al [41] numerical results in case 1 (Fig. 19a) at 0.1 m height. This error was obtained by Ciuman et al [41] numerical result at 26.5 ℃ and validation result at 25 ℃. At 0.6 m height, 4.4% absolute error was obtained for the results between validation and Ciuman et al [41] numerical results. The mean air temperature at 0.6 m

height was found to be 26 ℃ and 27.2 ℃ by validation and Ciuman et al. [41] numerical results respectively. In case 2 (Fig. 19b), Ciuman et al [41] measurements and validation results have showed low errors at height of 0.1 and 0.6 m with an absolute error range 0.4 and 0.58% respectively. Therefore, the validation results were proved to verify the measured results compared to the numerical solution of Ciuman et al. [41]. It is clearly observed that the height is directly proportional with the mean air temperature in (Fig. 19b, case 2) while it is inversely proportional as shown in (Fig. 19a). In case 3 (Fig. 15c), both numerical results of Ciuman et al. [41] and validation results showed to be directly proportional with height. Ciuman et al. [41] numerical results tend to be more precise with Ciuman et al. [41] measurement results compared to validation results. Generally, the error between validation and Ciuman et al. [41] measurement results showed to decrease from 5.45% to 0.9% at height from 0.1 to 1.7 m. In contrast, validation work showed to have absolute error with Ciuman et al. [41] numerical work in the range of 1.25 to 2.65% for all heights. This shows that both validation and Ciuman et al. [41] numerical work is in high precision compared to Ciuman et al. [41] experimental work. A figure that can be highlighted form (Fig. 19a, b and c) that the lowest error (0.9%) was obtained at 1.7 m for all cases between Ciuman et al. [41] measurements and validation results.

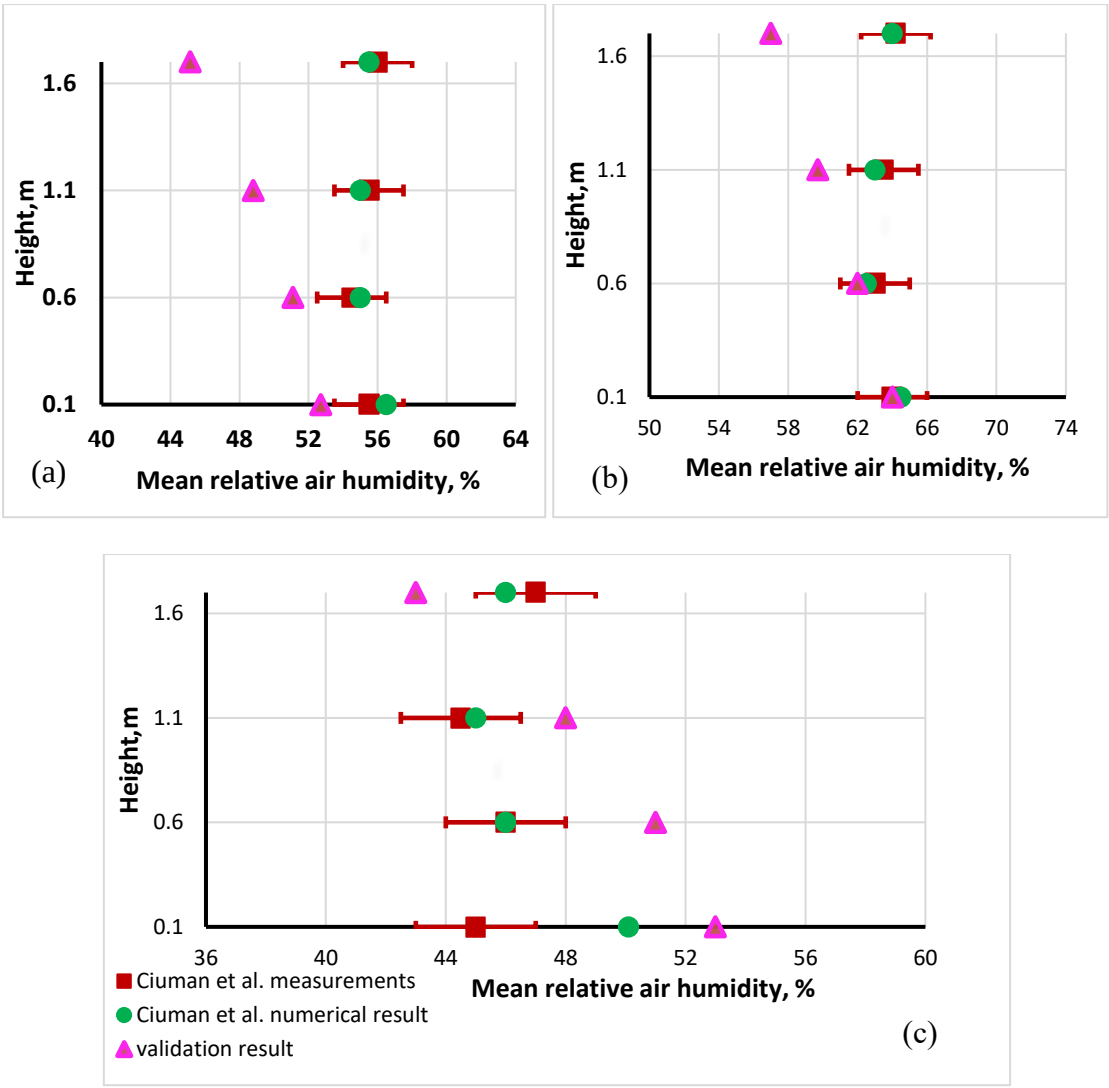

Figure 20. The comparison of results of Ciuman et al. measurements [41], Ciuman et al. numerical result [41] and validation result for mean relative humidity at four different heights for a) case 1, b) case 2, c) case 3.

The third air variable studied for this validation work was relative humidity which is essential in measuring the humidity levels in swimming pools. As shown in (Fig. 20a, case 1) RH decreases as height increases for validation results. The lowest RH was found to be 45.15% at height of 1.7 m which is 19% lower than the measurements and numerical simulation of Ciuman et al. [41]. The lowest absolute error 5.05% was achieved between validation and Ciuman et al. [41] measurement results at height of

0.1 m. While it was calculated 6.27% between validation and Ciuman et al. [41] numerical results at the same height 0.1 m. In case 2 (Fig. 20b, case 2), the error between validation results and other studies were reduced compared to case 1. At height 0.1 and 0.6 m, RH was obtained in range of 62 to 64 % and absolute error in the range of 0 to 1.59 % between all approaches. This indicates that RH were achieved for all approaches in case 2 is out of the recommended range for indoor condition and thermal comfort in swimming pools as per ASHRAE HVAC application chapter 6 indoor swimming pools. At height of 1.7 m, 57% RH was the highest mean relative humidity obtained by validation work with an error of 11.21% and 10.94% from measurement and numerical work of Ciuman et al. [41]. On the other hand, case 3 (Fig. 20b) showed high precision achievement between validation result and Ciuman et al. [41] numerical work. This can be observed at all heights where RH for validation results showed to be higher than Ciuman et al. [41] numerical result with 3% except for 1.7 m for height. The following mean relative humidity 53, 51 and 48% were obtained in validation result for heights of 0.1, 0.6 and 1.1 m respectively. In contrast, the absolute error between validation and Ciuman et al. [41] measurement was calculated 17.78, 10.87, 7.87 and 8.51% at heights of 0.1, 0.6, 1.1 and 1.7 m respectively.

In conclusion, the CFD analysis for validated model has proved its applicability to be used for this study through the small errors obtained in air temperature, air velocity and relative humidity. Air velocity was shown a high accuracy as it equates almost all velocities for the studies conducted via Ciuman et al. [41] at all heights. On the other hand, air temperature presented low errors compared to relative humidity for all cases but still not showing good results as air velocity. Relative humidity showed high deviation of validation result from Ciuman et al. [41] work at 0.1 m height for case 3 only. The validated model showed good results with low errors with Ciuman et al. [41]

measurement compared to Ciuman et al. [41] numerical results for all air flow parameters. In other words, validation work has shown to simulate the actual site conditions (Ciuman et al. [41] measurement) rather than Ciuman et al. [41] numerical work. However, the small error obtained between validation and Ciuman et al. [41] measurement results can be interpreted as minor errors that could be obtained in model creation and meshing process. In addition, it could be due to the under estimation of detailed information for internal fixtures such as radiator and lighting.

4.3 Air flow analysis for Qatar case

In this part, physical model will be analyzed thermally as the site being relocated in Qatar. Cooling load was calculated using several assumptions and inputs as provided in Table 1. The system output of HAP software was obtained, and cooling load was computed as per the parameters discussed in section 3.2 thermal loads. The output of HAP will be used in sizing and selectin the Air Handling Unit. A summary of HAP system output is demonstrated below in Table 16 Air System Sizing Summary.

Table 16 Air System Sizing Summary

Air System Specification (Numerical simulation inputs)	
Air flow rate (m^3/s)	1.314 (1.610 kg/s) – Summer 0.457 (0.560 kg/s) – Winter
Air temperature for Supply air inlet (℃)	19.8 ℃–Summer 21.5 ℃–Winter
Humidity ratio for for Supply air inlet (kgdw/kgda)	0.0088 kgdw/kgda –Summer 0.008 kgdw/kgda –Winter

Air flow rate, supply air temperature and humidity ratio from table 16 were used as an input to Ansys Fluent to conduct the numerical calculations. Air flow rate was verified by ASHRAE standard – HVAC application chapter 6 indoor swimming pools [46] using Air change per hour (ACH) rate. It was calculated 5 ACH which lays is within 4-

6 ACH as recommended by ASHRAE for spectators and swimming pool spaces. Verifying the calculated air flow had supported the use of boundary conditions (Table 16) as an input to the numerical calculation. Moreover, numerical calculation was done for summer and winter season cases utilizing different values of supply air temperature and humidity ratio values for each. Simulation in summer season was completed at 2000 iterations reaching 0.001 convergence criteria as discussed in section 3.3 CFD simulations. Average values for air velocity, air temperature and relative humidity were obtained for all heights 0.1, 0.6, 1.1 and 1.7 m where the deviation of results between each height was obtained to be from 0 to 5% deviation. In addition to that Air velocity, air temperature and RH Contours plot were presented at height 0.6 m as the sample from the domain in (Fig. 21a, b & c and Fig. 22a & b) for summer season and (Fig. 23a, b & c and Fig. 24a & b) for winter seasons.

4.2.1 Summer results

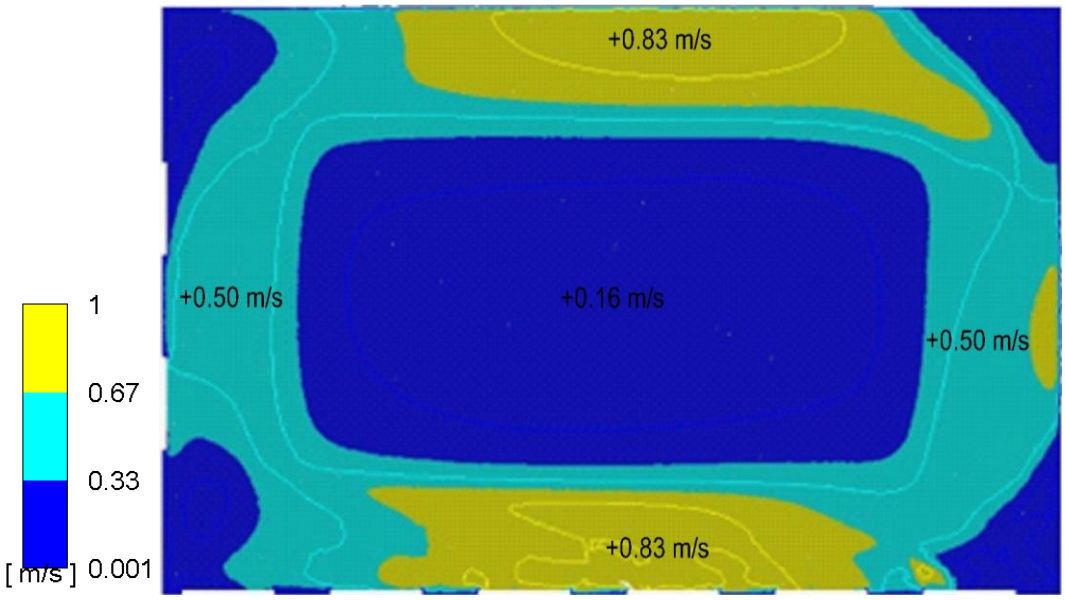

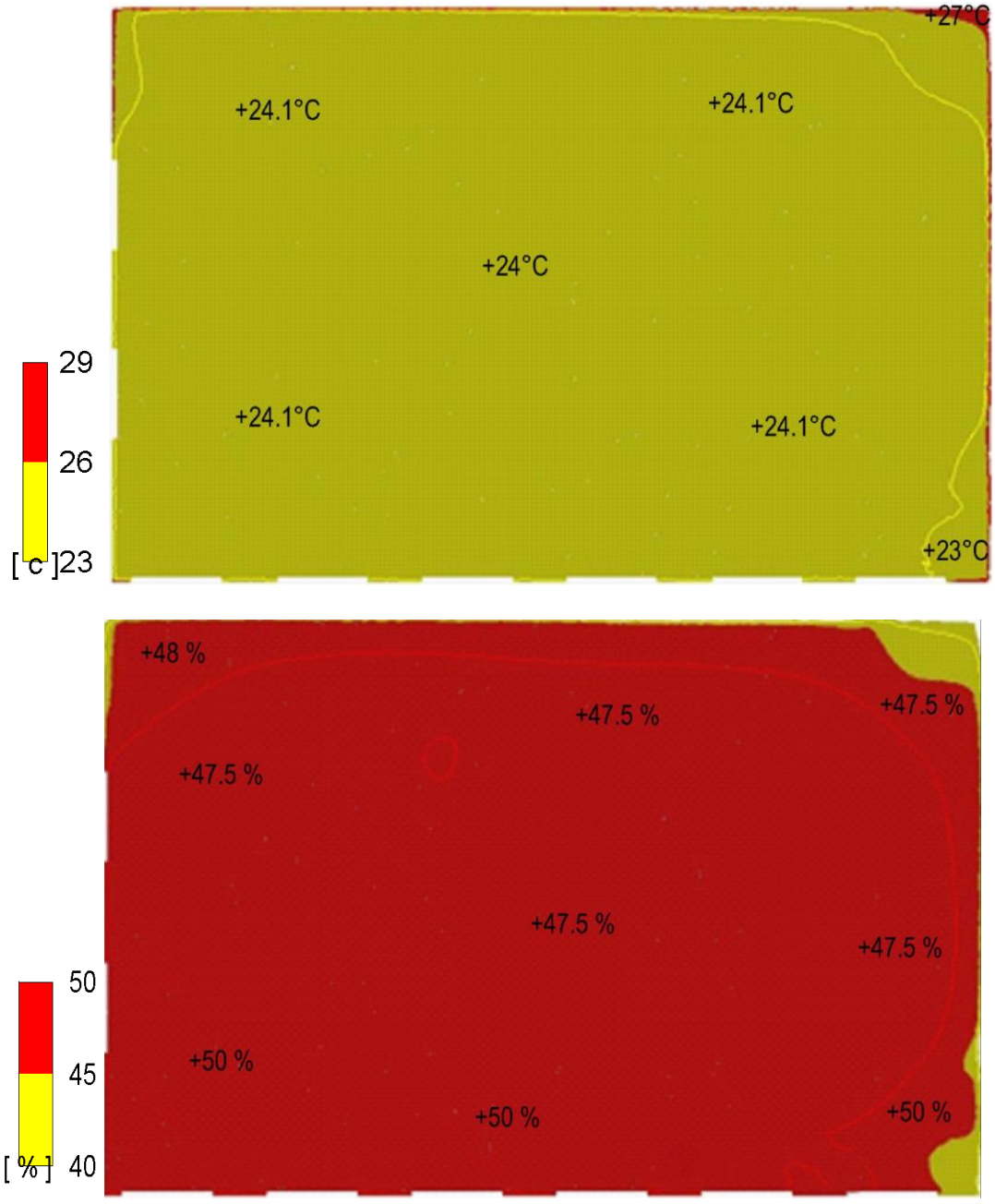

Figure 21. Contours plot for summer season at heigth 0.6 m: (a) Velocity contour plot (b) Temprature contour plot (c) Relative humidty contour plot.

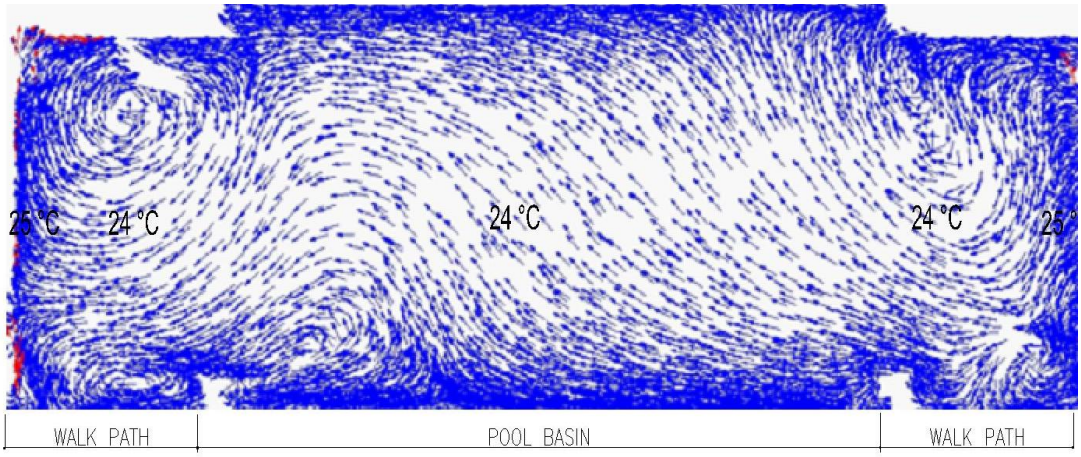

(a)

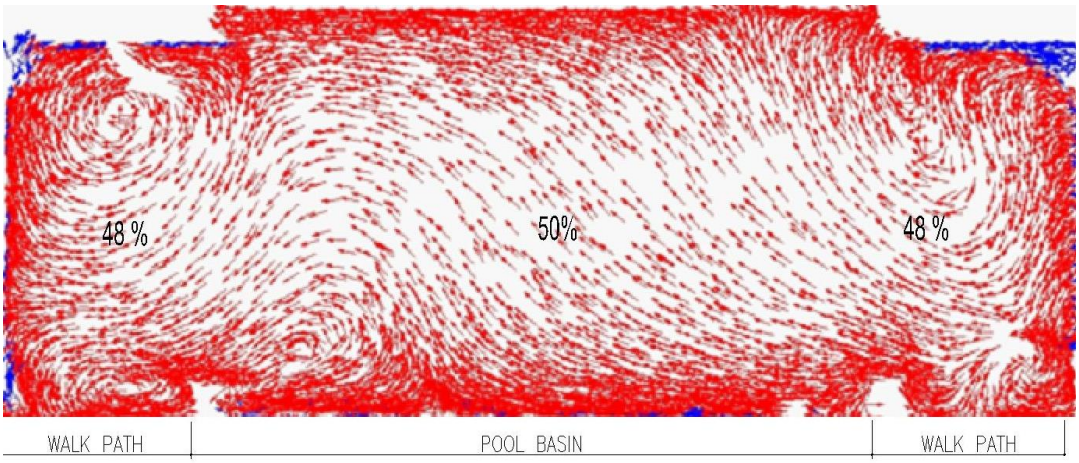

(b)

Figure 22. Velocity vector for summer season at sectional view of the swimming pool space: (a) Colored by Temprature (average temprature = 24°C) (b) Colored by Relative humidity (average RH%= 50%).

The Air conditioning system of swimming pool will be operated in cooling mode in summer conditions, so it is mandatory to maintain the required thermal comfort and indoor condition. In contrast, it will be operating in filtration mode in winter season as heating load was too low compared to cooling load as discussed in section 4.1 thermal loads. Velocity contours presented in to (Fig 21a) showed high velocity regions of 0.67 to 1 m/s around pool basin and an average velocity of 0.44 m/s for overall contour

planes (0.1, 0.6, 1.1 and 1.7 m). All velocity contour values showed to be within the acceptable range of velocities defined in thermal comfort criteria (0 to 1 m/s). Velocities contours located above pool basin were determined to cover a range from 0.1 to 0.3 m/s which is comfortable for swimmers as investigated by Elazm et al. [42] and Lebon et al. [33]. Most of the regions has laid between 0.3 to 0.5 m/s for an average velocity of 0.4 m/s as discussed in Caruso et al. results [43]. Moreover, velocity contours were investigated to be more turbulent compared to winter season as air flow rate supplied is higher in summer. All heights (0.1, 0.6, 1.1 and 1.7 m) showed the same results and contours distribution. In (Fig 21b and 22a) indoor temperature was found to be distributed uniformly among the space with an average air temperature of 24 ℃ for all contour planes (0.1, 0.6, 1.1 and 1.7 m). The variation between contour points was obtained ± 1℃ which is an indication of the uniformity of temperature inside the room. It was found that internal wall had a temperature of 30 ℃ and tends to decrease to 25 ℃ for air stream layers near to the wall. However, the computed average temperature showed to be within the recommended range of swimming pools (24 to 29 ℃). On the other hand, average relative humidity contours were calculated to be 47.3-47.7% for all heights as shown in (Fig 21c and 22b) except near walls 48% was achieved. RH of 47.5% was obtained for small areas near the corner walls of the space. Relative humidity contours indicate the effectiveness of air conditioning system in removing latent load from water evaporation process from pool basin. It was verified by ASHRAE standard (ASHRAE Handbook HVAC Application Chapter 6 indoor swimming pools) that the average 47.7 RH% is in the lower limit of the acceptable indoor conditions for swimming pools (40 to 60%). Lebon et. al. [33] presented high relative humidity results exceeding the range recommend ed by ASHRAE standards as the humidity ratio of supplied air was too high. Figure 22a and 22b, were produced to

clearly measure the uniformity of airflow distribution which has showed to be distributed uniformly in the whole space with no stagnant air locations being presented. In addition to that, it was verified that the thermal comfort conditions are achieved in the space with small variations. Thermal comfort criteria (PMV and PPD) have shown that high thermal comfort sensation was observed by occupants. As PMV was calculated +0.1 indicating neutral sensation for occupant. In other word, people have felt neither cold or hot environment. PPD% showed that 5.5% of people were dissatisfied with the indoor environment indicating almost 95% of occupant felt comfortable. A summary of indoor condition and thermal comfort results are shown below in Table 17.

Table 17 Summer season results summary

Height (m)	Average air temperature (℃)	Average air velocity (m/s)	Average relative humidity (%)	PMV index	PPD %
0.1	24	0.28	47.3	+0.13 (Neutral)	5.7
0.6	24	0.4	47.7	+0.1 (Neutral	5.5
1.1	24	0.44	47.7	+0.11 (Neutral)	5.5
1.7	24	0.49	47.5	+0.13 (Neutral)	5.6
Indoor conditions and Thermal Comfort limitations: Air temperature: 24< t_a <29℃ Air velocity: 0< v_a <1 m/s Relative humidity: 40 < RH% < 60 PMV index: +3 < PMV <- 3 PPD: 0 < PPD < 100%					

4.2.2 Winter results

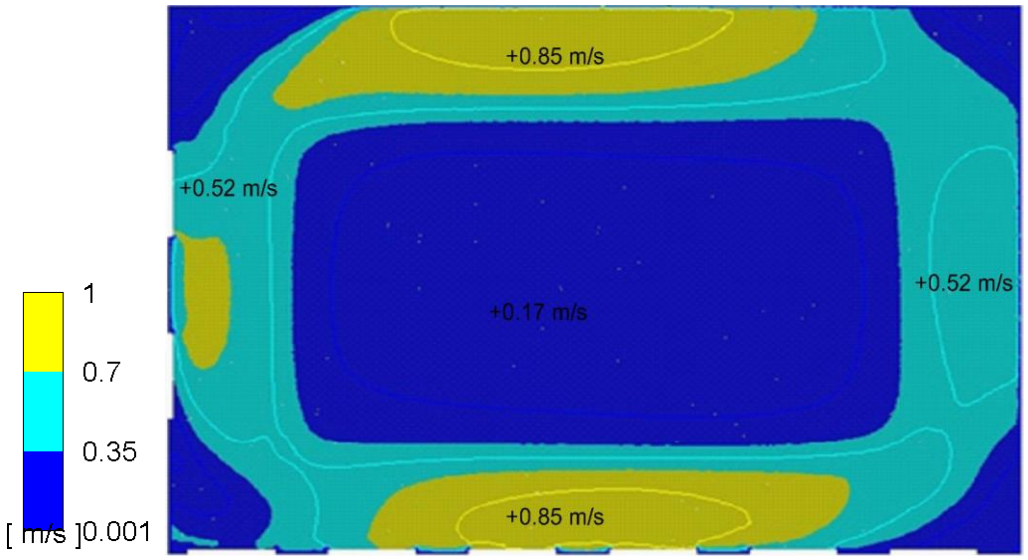

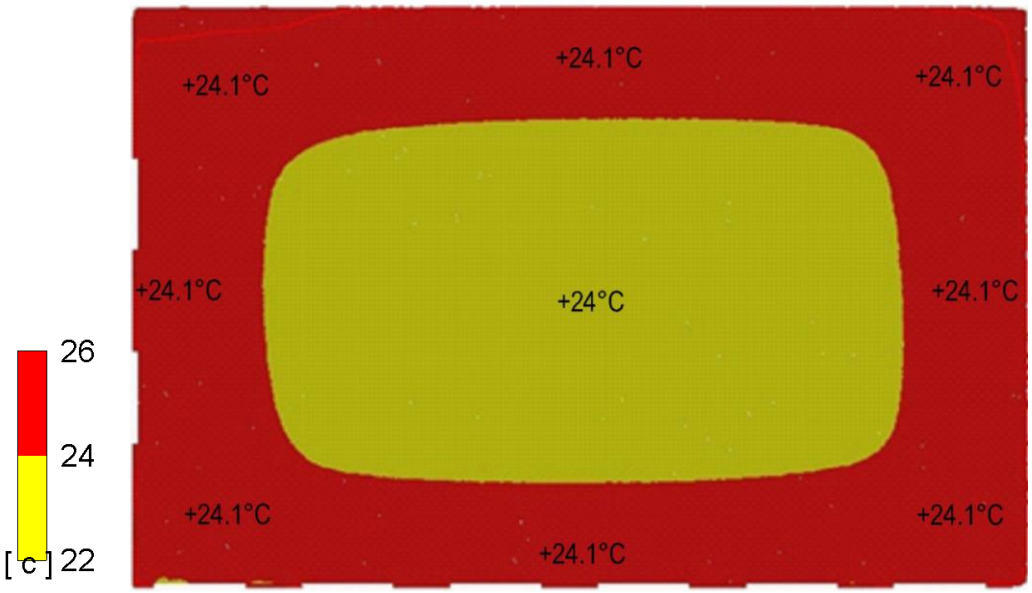

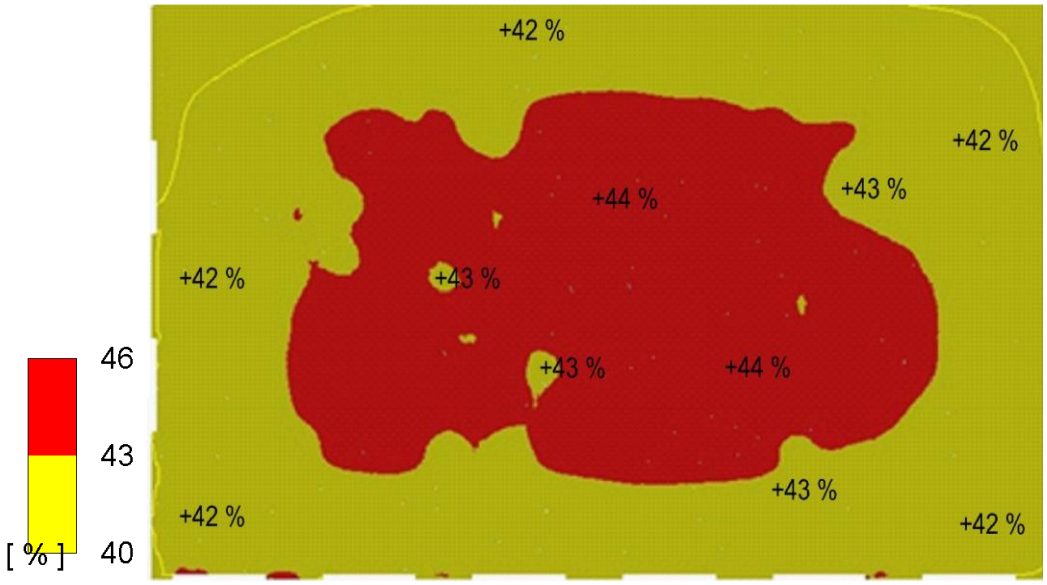

Figure 23. Contours plot for winter season at heigth 0.6 m: (a) Velocity contour plot (b) Temprature contour plot (c) Relative humidty contour plot.

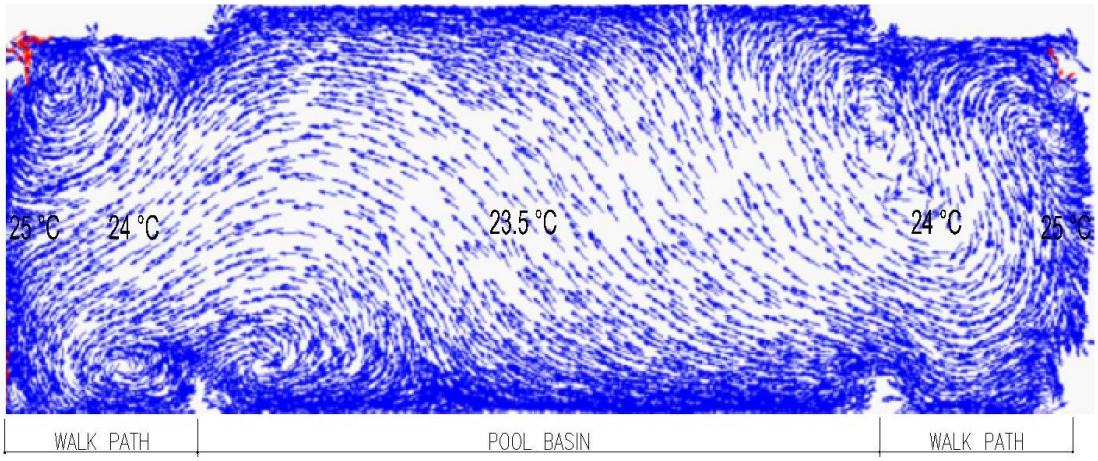

(a)

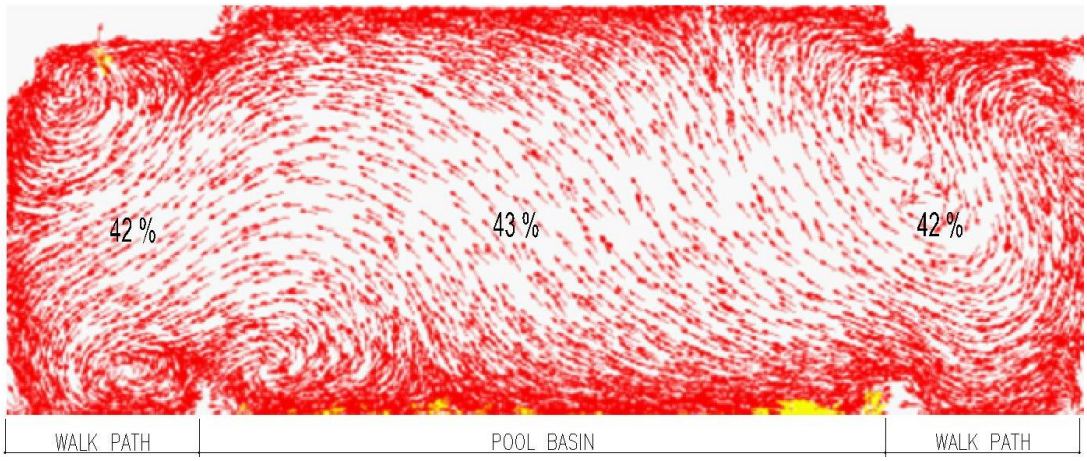

(b)

Figure 24. Velocity vector for winter season at sectional view of the swimming pool space: (a) Colored by Temprature (average temprature = 24.1℃) (b) Colored by Relative humidity (average RH%= 42.5%).

Air velocity is distributed uniformly in the space where no deviations were found across the contour plane, according to (Fig. 23a). Moreover, average velocities of 0.29, 0.45, and 0.49 m/s were calculated at heights of 0.1, 1.1, and 1.7m, respectively. From the edges of the pool basin toward the center, the air flow stream is seen to diminish with average velocity of 0.2 m/s. On the other hand, the air flow for walking path between

pool basin edge and room walls had a velocity of 0.4 m/s. The placement of the air inlets and outlets support the difference in air velocities obtained in walking path and pool basin area. The return air outlet is intended to exhaust air from the area above the pool basin, and the air inlets are intended to feed air above walking path area. 0.2 m/s Air velocity were computed in the corner areas as supply air inlets are far from these locations. The distribution of air velocity (average V = 0.4 m/s) in the whole domain showed to be within the range needed to use the thermal comfort model (0–1 m/s). Average Air temperature was calculated 24.1℃ for 0.1, 0.6 and 1.1 m planes while 24.2 ℃ was calculated for height 1.7 m. The analysis of temperature contours in sectional view showed walking path to have 24 ℃ while 23.5 ℃ was obtained for region above pool basin (Fig. 23b and 24a). The result if this analysis that were no evaporation of pool water surface was captured as temperature difference between air (23.5℃) and water surface (24 ℃) was reduced. On the other hand, the air temperature difference in the space was changing with 0.5 ℃ between walking space and pool basin area indicating the uniformity of air temperature contours. All boundary layers near room walls have shown air temperature of 25 ℃ as windows and walls are exposed to outdoor radiation load. As result of the computed contours, Air temperature showed to have distribution in the range of required indoor conditions (24 – 29℃) for swimming pools by ASHRAE standards. RH contours and sectional view displayed in (Fig. 23c and 24b) showed high humidity regions above pool basin as the moisture content increased. Moisture level increased above pool basin compared to other areas as water is evaporating from pool basin surface. The relative humidity showed to in the range of 43 to 46 % above pool basin while it was obtained in lower values of 42% for walk path area. The average relative humidity was found to be different between horizontal planes (0.1, 0.6, 1.1 and 1.7 m). It was calculated as 42.5% for contour plane 0.6 m while it

was computed as 42.6, 42.5 and 42.4% for 0.1, 1.1 and 1.7 m heights respectively. It is practical to have RH percentages lower than summer as outdoor conditions are different. In other words, supplied air conditions were varied via lowering supply humidity ratio in winter season which was achieved through the process of air conditioning system. In addition, lower RH values gives indication for lower moisture content in the space thus, avoiding condensation to occur on the structural elements such as windows and walls. Moreover, the results of RH contours plot showed to in the range of recommended RH by ASHRAE standards, 40-60% RH for swimming pools in winter season. In Figure 24a, 24b and 24c, the uniform distribution of air velocity, temperature and relative humidity discussed earlier in this section can be an indication of uniform thermal conditions (air velocity, temperature, and relative humidity). In addition to that, it was investigated that there are no stagnant air regions in all contours plane. Thermal comfort indices PMV and PPD were studied for the computed air variables (air velocity, temperature and relative humidity) for all planes. PMV was computed to be 0.74, 0.73, 0.75 and 0.76 for height of 0.1, 0.6, 1.1 and 1.7 m respectively. PMV calculation showed the occupant would feel slightly warm as it is approaching +1 (slightly warm). On the other hand, PPD% was determined as 17% for height at 1.1 and 1.7 m while 0.1 and 0.6 heights showed 16.7% dissatisfaction. Thus, 83% of occupants were satisfied with the indoor condition and felling comfortable in the space during the operation of Air conditioning system. A summary of all investigation for winter season are provided in Table 18 Winter season results summary.

Table 18 Winter season results summary

Height (m)	Average air temperature (°C)	Average air velocity (m/s)	Average relative humidity (%)	PMV index	PPD %
0.1	24.1	0.29	42.6	+0.73 (Slightly warm)	16.9
0.6	24.1	0.4	42.5	+0.74 (Slightly warm)	16.7
1.1	24.1	0.45	42.5	+0.75 (Slightly warm)	17
1.7	24.2	0.49	42.4	+0.76 (Slightly warm)	17

Table 4 Winter season results summary

Indoor conditions and Thermal Comfort limitations:
Air temperature: 24< t_a <29°C
Air velocity: 0< v_a <1 m/s
Relative humidity: 40 < RH% < 60
PMV index: +3 < PMV <- 3
PPD: 0 < PPD < 100%

CHAPTER 5: CONCLUSIONS AND FUTURE WORK

In this thesis, the thermal comfort and air variable properties were studied and analyzed for validated indoor swimming pool located in Qatar. Cooling load calculation was carried to obtain the boundary condition of supply air. All inlet, outlets and walls boundary conditions were defined in Ansys Fluent 19.2 to compute numerical simulation for a physical model of air-conditioned indoor swimming pool. Numerical grid was calculated with 1869824 elements using fine mesh and independent grid study. K-□ standard turbulence and species transport model were used in numerical calculation. The following was concluded as result of this study.

- Using 1.610 kg/s flow rate in summer and 0.560 kg/s in winter had achieved the recommended indoor conditions (50<RH<60% and 24 <t_a <29 ℃ in summer and 40<RH<60% and 24 <t_a <29 ℃ in winter) by ASHRAE HVAC Application Handbook Chapter 6 indoor swimming pool.
- Air temperature was obtained nearly 24 ℃ for all heights (at y=0.1,0.6,1.1 and 1.7 m). Air velocity showed to be 0.29, 0.4, 0.45 and 0.49 m/s for 0.1, 0.6, 1.1 and 1.1 m height respectively all year round. These values showed to be within the defined range of air velocities (0<v_a <1 m/s) as per Franger's model for thermal comfort analysis.
- In summer, Average relative humidity was obtained approximately 50% from contours plot (at y=0.1,0.6,1.1 and 1.7 m) which is in the recommended range of RH values as defined in ASHRAE HVAC Application Handbook Chapter 6 indoor swimming pool.
- In winter, average air velocity values were found to be equal to summer air velocities in all contour planes (0.1, 0.6, 1.1 and 1.7 m) while the average air

temperature was found to be higher by 0.1 ℃ for all temperature contour plots.

- Relative humidity was calculated to be approximately 42.5% in winter within the recommended value (40<RH<60%) by ASHRAE HVAC Application Handbook Chapter 6 indoor swimming pool.
- Reducing RH values to 42.5% is considered to be good practice of avoiding condensation process on structural elements as was discussed for natatoriums in ASHRAE HVAC Application Handbook Chapter 6 indoor swimming pool. It is scientifically described as vapor pressure become lower in the domain than the outdoor vapor pressure. Producing pressure differential across structural elements in which high pressure is obtained outdoor and low pressure is obtained indoor. Thus, indoor airflow will be unable to reach the room internal walls das flow will not transfer from low pressure to high pressure. 42.5% could be achievable all year round as low moisture content is obtained indoor.
- The second part of thermal comfort assessment was measuring the sensation of occupant using the achieved indoor conditions in summer and winter by simulation. Thermal sensation of occupant was determined to be neutral in summer and slightly warm in winter. PMV was calculated as +0.13 (Nearly neutral) for all heights in summer period and +0.73-0.76 for all heights in winter period.
- In addition to PMV, PPD index was studied where 16-17% of occupants were dissatisfied from the indoor environment in winter season. It can be derived from the calculated low RH% value, however it was vital to achieve lower value to reduce moisture content. Thereby, avoiding condensation and deterioration of structural elements in the room enclosure. On the other hand, PPD=5.5% occupant felt dissatisfied with indoor conditions in summer season indicating the good distribution of air flow and the effectiveness of AC system in providing comfort to

occupants. In overall, it can be summarized from this study that the verified supply air flow conditions have achieved both thermal comfort and acceptable moisture content to overcome any condensation occurrence in summer and winter for hot and humid outdoor conditions of Qatar.

In this thesis work, thermal analysis is conducted using numerical CFD simulation for swimming pool in desert region using ASHRAE and other standards in determining the recommended indoor conditions for thermal comfort. Thermal analysis was done based on cooling load and air flow calculation. Varying air flow from 4 and 6 ACH (Air Change per Hour) is recommended by ASHRAE in ASHRAE HVAC Application Handbook Chapter 6 indoor swimming pool.. However, 5 ACH was obtained from air flow and cooling load calculation have produced optimum results for the indoor conditions and thermal comfort in this case study. It could be diverted and air flow calculation is obtained using 4 or 6 ACH. Then use the obtained air flow in numerical calculation as a new approach to obtain new indoor conditions and thermal comfort results. Even though, 5 ACH showed to be acceptable for doing the thermal analysis for this study but it is suggested to do experimental work as a part from advanced work to this area of study. Firstly, it will validate the air variable contours and the verified supplied air flow conditions by ASHRAE standards. Secondly, thermal comfort survey would be conducted as apart from the experimental work and all collected votes would be validated by the calculated indices (PMV and PPD) from Finger's thermal comfort model. Moreover, latent load of Pool water evaporation shows to highly share a part in the total thermal load. This requires efficient and sufficient HVAC system that can remove such loads. Therefore, adding or removing humidifiers and dehumidifiers can have critical contribution in the energy demand of HVAC system. Therefore, Energy demand is considered to be important part and hot topic from HVAC system

applications for indoor swimming pools. Conducting energy analysis for HVAC system is critical and challengeable to achieve thermal comfort using sustainable HVAC system in sever outdoor hot and humid outdoor conditions of Qatar.

REFERENCES

[1] Ramírez H, Jiménez-Cabas J, Bula A. Experimental data for an air-conditioning system identification. Data Br 2019;25:104316.

[2] Mikeska T, Fan J. Full scale measurements and CFD simulations of diffuse ceiling inlet for ventilation and cooling of densely occupied rooms. Energy Build 2015;107:59–67.

[3] Abadie MO, De Camargo MM, Mendonça KC, Blondeau P. Improving the prediction of zonal modeling for forced convection airflows in rooms. Build Environ 2012;48:173–82.

[4] Ghanta N, Kongoletos J, Glicksman L. Comfort control and improved thermostat location in conference rooms and academic working spaces. Build Environ 2021;205:108192.

[5] Wang H, Liu L, Liu L, Cheng Q. Performance analysis of different air conditioning systems in apartment buildings under different climates in China. Int J Refrig 2022.

[6] Ekici C. A review of thermal comfort and method of using Fanger's PMV equation. 5th Int. Symp. Meas. Anal. Model. Hum. Funct. ISHF, 2013, p. 61–4.

[7] Cao Q, Liu M, Li X, Lin C-H, Wei D, Ji S, et al. Influencing factors in the simulation of airflow and particle transportation in aircraft cabins by CFD. Build Environ 2022;207:108413.

[8] Indraganti M, Boussaa D. An adaptive relationship of thermal comfort for the Gulf Cooperation Council (GCC) Countries: The case of offices in Qatar. Energy Build 2018;159:201–12.

[9] Yin H, Guo H, Lin Z, Zeng B. CFD simulation of air-conditioning system in the

public area of a metro station and research on energy-saving operation scheme. 2017 2nd Int. Conf. Civil, Transp. Environ. Eng. (ICCTE 2017), Atlantis Press; 2017, p. 699–705.

[10] Mboreha CA, Jianhong S, Yan W, Zhi S, Yantai Z. Investigation of thermal comfort on innovative personalized ventilation systems for aircraft cabins: A numerical study with computational fluid dynamics. Therm Sci Eng Prog 2021;26:101081.

[11] Ghani S, Bakochristou F, ElBialy EMAA, Gamaledin SMA, Rashwan MM, Abdelhalim AM, et al. Design challenges of agricultural greenhouses in hot and arid environments – A review. Eng Agric Environ Food 2019;12:48–70. https://doi.org/10.1016/j.eaef.2018.09.004.

[12] Ghani S, El-Bialy EMAA, Bakochristou F, Mohamed Rashwan M, Mohamed Abdelhalim A, Mohammad Ismail S, et al. Experimental and numerical investigation of the thermal performance of evaporative cooled greenhouses in hot and arid climates. Sci Technol Built Environ 2020;26:141–60. https://doi.org/10.1080/23744731.2019.1634421.

[13] Xu J, Li Y, Wang RZ, Liu W, Zhou P. Experimental performance of evaporative cooling pad systems in greenhouses in humid subtropical climates. Appl Energy 2015;138:291–301. https://doi.org/10.1016/j.apenergy.2014.10.061.

[14] Kittas C, Bartzanas T, Jaffrin A. Greenhouse evaporative cooling: measurement and data analysis. Trans ASAE 2001;44:683.

[15] Lertsatitthanakorn C, Rerngwongwitaya S, Soponronnarit S. Field experiments and economic evaluation of an evaporative cooling system in a silkworm rearing house. Biosyst Eng 2006;93:213–9. https://doi.org/10.1016/j.biosystemseng.2005.12.003.

[16] Tazima Y. The silkworm: an important laboratory tool 1978.

[17] Kittas C, Bartzanas T, Jaffrin A. Greenhouse evaporative cooling: measurement and data analysis. Int. Conf. British-Israeli Work. Greenh. Tech. Towar. 3rd Millenn. 534, 2000, p. 67–74.

[18] Newman JP. Container nursery production and business management manual. vol. 3540. UCANR Publications; 2014.

[19] DAYIOĞLU MA, SİLLELİ HH. Performance analysis of a greenhouse fan-pad cooling system: gradients of horizontal temperature and relative humidity. J Agric Sci 2015;21:132–43.

[20] Worley JW. Greenhouses: heating, cooling and ventilation. University of Georgia; 2009.

[21] Leyva R, Constán-Aguilar C, Sánchez-Rodríguez E, Romero-Gámez M, Soriano T. Cooling systems in screenhouses: Effect on microclimate, productivity and plant response in a tomato crop. Biosyst Eng 2015;129:100–11.

[22] Sonneveld PJ, Swinkels G, Kempkes F, Campen JB, Bot GPA. Greenhouse with an integrated NIR filter and a solar cooling system. Int. Symp. Greenh. Cool. 719, 2006, p. 123–30.

[23] Al-Mulla YA, Al-Balushi M, Al-Busaidi H, Al-Mahdouri A, Kittas C, Katsoulas N. Analysis of microclimate and cucumber fruit yield in a screenhouse and an evaporatively cooled greenhouse in a semi-arid location. Trans ASABE 2018;61:619–29. https://doi.org/10.13031/trans.12144.

[24] Albright LD, Seginer I, Marsh LS, Oko A. In situ thermal calibration of unventilated greenhouses. J Agric Eng Res 1985;31:265–81.

[25] Perdigones A, García JL, Pastor M, Benavente RM, Luna L, Chaya C, et al. Effect of heating control strategies on greenhouse energy efficiency:

Experimental results and modeling. Trans ASABE 2006;49:143–55.

[26] Perdigones A, Pascual V, García JL, Nolasco J, Pallares D. Interactions of crop and cooling equipment on greenhouse climate. Int. Conf. Sustain. Greenh. Syst. 691, 2004, p. 203–8.

[27] Perdigones A, García JL, Romero A, Rodríguez A, Luna L, Raposo C, et al. Cooling strategies for greenhouses in summer: Control of fogging by pulse width modulation. Biosyst Eng 2008;99:573–86. https://doi.org/10.1016/j.biosystemseng.2008.01.001.

[28] Morsi SAJ, Alexander AJ. An investigation of particle trajectories in two-phase flow systems. J Fluid Mech 1972;55:193–208.

[29] Ferziger JH, Perić M, Street RL. Computational methods for fluid dynamics. vol. 3. Springer; 2002.

[30] Kim K, Yoon JY, Kwon HJ, Han JH, Eek Son J, Nam SW, et al. 3-D CFD analysis of relative humidity distribution in greenhouse with a fog cooling system and refrigerative dehumidifiers. Biosyst Eng 2008;100:245–55. https://doi.org/10.1016/j.biosystemseng.2008.03.006.

[31] Ishii M, Sase S, Moriyama H, Kurata K, Ikeguchi A, Kubota C, et al. The effect of evaporative fog cooling in a naturally ventilated greenhouse on air and leaf temperature, relative humidity and water use in a semiarid climate. Proc. Int. Symp. Greenh. Cool., International Society for Horticultural Science; 2006, p. 491–8.

[32] Ishii M, Okushima L, Moriyama H, Sase S, Takakura T, Kacira M. Effects of Natural Ventilation Rate on Temperature and Relative Humidity in a Naturally Ventilated Greenhouse with High Pressure Fogging System. n.d.

[33] Lebon M, Fellouah H, Galanis N, Limane A, Guerfala N. Numerical analysis

and field measurements of the airflow patterns and thermal comfort in an indoor swimming pool: a case study. Energy Effic 2017;10:527–48. https://doi.org/10.1007/s12053-016-9469-0.

[34] Daoud A, Galanis N. Calculation of the Thermal Loads of an Ice Rink Using a Zonal Model and Building Energy Simulation Software. ASHRAE Trans 2006;112.

[35] Limane A, Fellouah H, Galanis N. Simulation of airflow with heat and mass transfer in an indoor swimming pool by OpenFOAM. Int J Heat Mass Transf 2017;109:862–78. https://doi.org/10.1016/j.ijheatmasstransfer.2017.02.030.

[36] Limane A, Fellouah H, Galanis N. Three-dimensional OpenFOAM simulation to evaluate the thermal comfort of occupants, indoor air quality and heat losses inside an indoor swimming pool. Energy Build 2018;167:49–68. https://doi.org/10.1016/j.enbuild.2018.02.037.

[37] Addas MJ, Chaudhuri-Oslomet A, Kampel-Multiconsult W, Og M, Mohamed O, Addas J. Improving the ventilation in passive house swim-ming pool: a case study of Åfjord swimming pool. n.d.

[38] Liu D, Zhao F-Y, Yang H, Chen J, Ye C. Probability adjoint identification of airborne pollutant sources depending on one sensor in a ventilated enclosure with conjugate heat and species transports. Int J Heat Mass Transf 2016;102:919–33.

[39] Li Z;, Heiselberg PK. CFD Simulations for Water Evaporation and Airflow Movement in Swimming Baths. 2005.

[40] Spesifikasjon for svømmeanlegg. 2010.

[41] Ciuman P, Lipska B. Experimental validation of the numerical model of air, heat and moisture flow in an indoor swimming pool. Build Environ 2018;145:1–13. https://doi.org/10.1016/j.buildenv.2018.09.009.

[42] Elazm MMA, Shahata AI. Numerical and field study of the effect of air velocity and evaporation rate on indoor air quality in enclosed swimming pools. Drag Reduct Veloc Profiles Distrib Crude Oil Flow Spiral Pipes 2015:97.

[43] Caruso G, De Santoli L, Mariotti M. Ventilation Design in Large Enclosures for Sports Events using CFD: the Halls of the "Città dello Sport" in Rome. n.d.

[44] Ashrae. ASHRAE Pocket Guide for Air Conditioning, Heating, Ventilation, Refrigeration. ASHRAE; 2018.

[45] Persily A, Musser A, Emmerich SJ. Modeled infiltration rate distributions for US housing. Indoor Air 2010;20:473–85.

[46] Janssen J. Ventilation for acceptable indoor air quality. ASHRAE J 1989;31:40–8.

[47] Sharp TR. 2019 ASHRAE Handbook: HVAC Applications-Chapter 37-Energy Use and Management. Oak Ridge National Lab.(ORNL), Oak Ridge, TN (United States); 2020.

[48] Handbook-Fundamentals A. Residential Cooling and Heating Load Calculations 2001.

[49] Sleiti AK, Al-Ammari WA, Arshad R, El Mekkawy T. Energetic, economic, and environmental analysis of solid oxide fuel cell-based combined cooling, heating, and power system for cancer care hospital. Build. Simul., vol. 15, Springer; 2022, p. 1437–54.

[50] Sleiti A, Salehi M, Idem S. Detailed velocity profiles in close-coupled elbows—Measurements and computational fluid dynamics predictions (RP-1682). Sci Technol Built Environ 2017;23:1212–23.

[51] Salehi M, Idem S, Sleiti A. Experimental determination and computational fluid dynamics predictions of pressure loss in close-coupled elbows (RP-1682). Sci

Technol Built Environ 2017;23:1132–41.

[52] Darwish M, Moukalled F. The finite volume method in computational fluid dynamics: an advanced introduction with OpenFOAM® and Matlab®. Springer; 2021.

[53] Sleiti AK, Zhai J, Idem S. Computational fluid dynamics to predict duct fitting losses: Challenges and opportunities. HVAC&R Res 2013;19:2–9.

[54] Navier-Stokes Equations n.d.

[55] Salehi M, Sleiti AK, Idem S. Study to identify computational fluid dynamics models for use in determining HVAC duct fitting loss coefficients. Sci Technol Built Environ 2017;23:181–91.

[56] Sleiti AK, Kapat JS. Comparison between EVM and RSM turbulence models in predicting flow and heat transfer in rib-roughened channels. J Turbul 2006;7. https://doi.org/10.1080/14685240500499343.

[57] Markov D. Practical evaluation of the thermal comfort parameters. Annu Int Course Vent Indoor Clim Avangard, Sofia 2002:158–70.

[58] Thevenard DJ, Humphries RG. The calculation of climatic design conditions in the 2005 ASHRAE Handbook-Fundamentals. ASHRAE Trans 2005;111:457.

[59] Ashrae A. Standard 55-2013: Thermal environmental conditions for human occupancy. Am Soc Heating, Refrig Air-Conditioning Eng Inc Atlanta 2013.

[60] American Society of Heating R and A-CE. 1997 ASHRAE Handbook: Fundamentals. ASHRAE; 1997.